Universidad de Concepción
Facultad de Ingeniería
Departamento de Ingeniería Química

Magíster En Ciencias De La Ingeniería Con Mención En Ingeniería Química

Estudio mecanístico mediante espectroscopía infrarroja in situ de la oxidación selectiva de metanol sobre catalizadores de molibdeno y vanadio

por

Bastián Alexis Fuentes Soto

Guía

Profesor Alejandro Karelovic Burotto

Noviembre 2025
Concepción, Chile

Agradecimientos

“No llores porque terminó, sonríe porque sucedió” Esta cita fue una de las frases que más me marcó este 2025 y refleja perfectamente cómo me siento al cerrar este capítulo en CarboCat. Pero antes de agradecer a este maravilloso grupo de personas, quiero reconocer a quienes me permitieron tomar este camino inesperado y hermoso hacia convertirme en Master en Ciencias de la Ingeniería con mención en Ingeniería Química.

Gracias a mis padres, por su amor incondicional, su paciencia y por apoyarme en cada paso de este camino. Saber que estaban tranquilos y felices con la ruta que había elegido me permitió avanzar con confianza, sin importar cuántas dificultades aparecieran en el camino.

Gracias a mi querida Catalina, quien me dio el impulso final para postular al programa de magíster y que estuvo a mi lado durante todo el proceso. Gracias por escuchar mis quejas, mis alegrías, mis interminables quejas y aún más quejas. Fuiste realmente un pilar fundamental que me ayudó a respirar cada vez que lo necesité. Gracias por despejar mi mente cuando estaba saturado de resultados e isótopos. Me diste calma cuando más lo necesitaba.

A mis fieles amigos del colegio, gracias por ser un grupo capaz de distraerme incluso en los momentos más tensos. Sinceramente, salir con ustedes cada viernes por medio fue una de las rutinas más “saludables” que tuve durante estos años, y se convirtió en un punto clave a lo largo de todo este proceso.

Al llegar a Carbocat, es imposible no describir a este grupo como una familia. Gracias, Vero, por todo. Estoy seguro de que todos en el laboratorio coinciden en que este lugar simplemente no funcionaría sin ti. Gracias por el apoyo infinito que brindas a cada uno de nosotros. Gracias, Naxis, quien no solo se convirtió en mi mejor amiga en el laboratorio, sino también en una hermana para mí. Gracias por hacer equipo conmigo en todo tipo de cosas en el lab, por las idas espontáneas por helado durante la semana, por tu apoyo durante el trabajo experimental y por cada conversación que compartimos durante estos dos años.

También quiero agradecer a mis estudiantes de tesis de pregrado, o mis *minions*: Rodrigo, Matías, Fernando, Camilo y Margarita. Colaborar con ustedes en el laboratorio 413 me enseñó cosas nuevas, abrió nuevas perspectivas y me regaló innumerables momentos de alegría y distracción. Espero haber dejado algo significativo en cada uno de ustedes. Al mismo tiempo, no quiero dejar fuera a todos los estudiantes que también nos acompañaron durante estos dos años. Fue realmente grato coincidir con ustedes en el laboratorio.

A mi dúo cervecero, Gabriel y Pancho, gracias por cada discusión, cada café y cada cerveza. Cada momento enriqueció este proceso tanto en lo académico como en lo personal.

A los profesores del laboratorio, Romel, Tati, X y Luis, gracias por crear el ambiente cálido y positivo que define a Carbocat. Su guía, su retroalimentación constructiva y su cuidado en la selección de las personas que integran el grupo hacen de este un lugar especial.

A las nuevas generaciones de Carbocat, mis palabras de ánimo: no duden en pedir ayuda. Los experimentos fallan, las cosas se rompen y los días pueden ser duros, pero todo problema tiene solución. Por favor, mantengan a Carbocat como el espacio cálido y colaborativo que es.

Finalmente, gracias Alejandro, por estos tres años de trabajo juntos, comenzando en marzo de 2022 y terminando ahora, a fines de 2025. Fueron los años más disfrutables de mi formación. Gracias por confiarme uno de tus temas de investigación más desafiantes, por darme claridad y calma después de cada reunión y por confiarme todo el equipamiento nuevo del laboratorio. Espero que el IR y el MS sobrevivan después de que me vaya. Gracias por apostar por mí y por darme la oportunidad de convertirme en master en ingeniería química. No existen palabras para expresar mi gratitud.

Y así, todo lo que puedo decir ahora es: no llores porque terminó, sonríe porque sucedió.

Acknowledgements

“Don’t cry because it’s over, smile because it happened.” This phrase was one of the quotes that marked me the most in 2025, and it perfectly reflects how I feel as I close this chapter at Carbocat. But before thanking this wonderful group of people, I want to acknowledge those who allowed me to take this unexpected and beautiful path toward becoming a Master of Science in Engineering with a mention in Chemical Engineering.

Thank you to my parents, for your unconditional love, patience, and for supporting me through every step of this journey. Knowing that you were calm and happy with the path I had chosen allowed me to move forward with confidence, no matter how many difficulties showed up along the way.

Thank you to my lovely Catalina, who gave me the final push to apply to the master’s program, and who stayed by my side through the entire process. Thank you for listening to me, my complaints, my joys, my endless complaints, and even more complaints. You were truly a fundamental pillar that helped me breathe whenever I needed it. And thank you for clearing my mind when it was overflowing with results and isotopes. You gave me calm when I needed it most.

To my loyal school friends, thank you for being the group capable of distracting me even in the tensest moments. Honestly, going out with you every other Friday was one of the “healthiest” routines I had during these years, and it became a crucial point of balance throughout this entire process.

Reaching Carbocat, it is impossible not to describe this group as a family. Thank you, Vero, for everything. I am sure everyone in the lab agrees that this place simply would not function without you. Thank you for the endless support you give each one of us. Thank you Naxis, who became not only my best friend in the lab but a sister to me. Thank you for teaming up with me for all kinds of things in the lab, for the spontaneous ice cream runs during the week, for your warm support during the experimental work, and for every conversation we shared over these two years.

I also want to thank my undergraduate thesis students or my minions: Rodrigo, Matías, Fernando, Camilo, and Margarita. Collaborating with you in 413 laboratory taught me new things, opened new perspectives, and gave me countless moments of joy and distraction. I hope I have left something meaningful with each of you. At the same time, I do not want to leave out all the students who still accompanied us throughout these two years. It was genuinely nice to overlap with you in the lab.

To my beer duo, Gabriel and Pancho, thank you for every discussion, every coffee, and every beer. Each moment enriched this process both academically and personally.

To the professors of the lab, Romel, Tati, X and Luis, thank you for creating the warm and positive environment that defines Carbocat. Your guidance, your constructive feedback, and your care in selecting the people who join the group make this place special.

To the new generations of Carbocat, my words of encouragement: do not hesitate to ask for help. Experiments fail, things break, and days can be tough, but every problem has a solution. And please, keep Carbocat the warm and collaborative space it is.

Finally, thank you Alejandro, for these three years of work together, starting in March 2022 and ending now, in late 2025. These were the most enjoyable years of my education. Thank you for trusting me with one of your most challenging research topics, for giving me clarity and calm after every meeting, and for trusting me with all the new equipment in the lab. I hope the IR and MS survive after I leave. Thank you for betting on me and giving me the opportunity to become a master's in chemical engineering. There are no words to express my gratitude.

And so, all I can say now is: Don't cry because it's over, smile because it happened.

Abstract

Methanol oxidative dehydrogenation on titania supported metal oxide catalysts was studied to clarify different mechanistic proposals reported in the literature. Operando spectroscopic and isotopic transient experiments under controlled reaction conditions, combined with correlations between catalyst structure and product distribution, revealed how the nature of redox sites governs the methyl formate formation and integrates the reaction pathways into a coherent framework.

Sub-monolayer MoO_3/TiO_2 and V_2O_5/TiO_2 catalysts, dominated by highly dispersed interfacial M–O–Ti linkages (M = Mo, V), stabilize formate-type intermediates which favor methyl formate production through the formate–mediated route. In contrast, catalysts featuring crystalline M–O–M domains promote the hemiacetal intermediate, where less–stabilized intermediates lead directly to methyl formate and dimethoxymethane formation. These results indicate a common mechanistic framework for both Mo– and V–based systems, in which the dominant pathway is selectively expressed depending on the nature and distribution of redox sites rather than on the metal identity itself.

Isotopic labeling and transient experiments rule out extensive methoxy exchange and the Tishchenko pathway for methyl formate formation, under the studied conditions. Differences in intermediates stabilization, active sites distribution, and kinetic isotope effects account for the observed variations in reaction orders and selectivity.

Overall, the study demonstrates that the formation of oxygenates in methanol oxidative dehydrogenation critically depends on the type of redox site involved, establishing a structural – mechanistic framework that rationalizes the behavior of MoO_3/TiO_2 and V_2O_5/TiO_2 catalysts and can be extended to other reducible oxide systems engaged in selective oxidation reactions.

Table of contents

Introduction

Currently, the catalysis community is focused on solving energy and chemical problems such as H_2 storage[1], the sustainable production of chemical fuels[2], and the valorization of CO_2 into high-value chemicals[3]. In this context, Olah[4] proposed the concept of "methanol economy", positioning methanol as key molecule to reduce our dependence on fossil fuels. Moreover, methanol is a promising H_2 carrier[1] and serves as a C_1 building block of many other compounds[5].

One of the reactions in which methanol acts as a building molecule is the methanol partial oxidation or oxidative dehydrogenation of methanol (ODH). This reaction produces compounds such as formaldehyde (HCHO, FA), dimethoxymethane ($CH_3OCH_2OCH_3$, DMM), and methyl formate ($HCOOCH_3$, MF), among others[6].

Formaldehyde is one of the products obtained industrially through the partial oxidation of methanol via the *Formox* process. Currently, the process is mainly carried out over Fe–Mo mixed oxide catalyst at 250 – 400°C, at atmospheric pressure in excess air, obtaining a high yield to FA with near complete conversion[7]. In the *Formox* process methanol vaporized in the process gas and passed into a tubular reactor. Subsequently, the mixture at the reactor outlet, composed mainly of formaldehyde and water, is cooled and conducted into a multi-stage absorption system, where the formaldehyde is separated and recovered[7].

On the other hand, the industrial methyl formate production proceeds via liquid–phase methanol carbonylation at 80°C, 40 bar pressure, and using sodium methoxide as catalyst. Although this method can achieve high selectivity (but at low conversion), they often suffer from issues related to corrosion, catalyst moisture sensitivity, and environmental concerns due to the use of toxic CO feedstocks and liquid-phase operations.[8]

Under this context, the production of methyl formate via heterogeneous catalysis in the gas phase and in a continuous process is an attractive alternative. Nevertheless, most metal oxide catalysts are not active and/or selective enough from the industrial standpoint, it is still highly demanding to develop efficient catalysts for the oxidative dehydrogenation of methanol[8].

To address this challenge, extensive research has been devoted to understanding the oxidative dehydrogenation of methanol over various oxide catalysts[9–12]. Transition metal oxides, such as bulk and supported molybdenum, vanadium, and ruthenium, have been particularly employed due to their high redox activity and their ability to participate in Mars-van Krevelen cycles[13] necessary for formaldehyde formation. In this mechanism, lattice oxygen atoms from the oxide surface are involved in the oxidation of methanol, leading to the formation of FA, followed by catalyst reoxidation with gas-phase oxygen[14]. Within this redox cycle, the

first dehydrogenation of the methoxy group is widely accepted to be the rate-determining step (RDS) in the overall methanol ODH [6,12,15,16].

However, the subsequent steps to form DMM and MF remain under debate, with no clear consensus regarding the intermediates involved. Previous works[15–19] suggest that dioxymethylene (O–CH_2–O) and formate (HCOO) are the intermediates in a shared reaction pathway. This pathway is supported by FTIR-operando studies. Busca et al.[16–18], studying with vanadium-based catalysts, observed that dioxymethylene is the stable form of adsorbed formaldehyde. This species can react with two CH_3OH molecules to produce $CH_3OCH_2OCH_3$ or continues to dehydrogenate on the surface to form formate species, which can then react with CH_3OH to yield $HCOOCH_3$[19], or produce complete oxidation products such as CO and CO_2.

On the other hand, hemiacetal (CH_3OCH_2OH) has also been proposed as the intermediate leading to the formation of DMM and MF[12,20–23]. In an earlier study, Wachs and Madix[20] observed that a complex between HCHO and CH_3OH forms $HCOOCH_3$ more easily than a complex of CH_3OH and HCOOH (as a precursor for formates species). Later, different researchers[12,24,25] supported the idea that hemiacetal is the intermediate, based on the observed relation between DMM and MF. $CH_3OCH_2OCH_3$ is a reversible product in equilibrium with CH_3OCH_2OH, which can undergo dehydrogenation at high temperatures to form $HCOOCH_3$. Additionally, Iglesia and Liu[12] observed that the selectivity between DMM and MF may change depending on the presence of Brønsted acid sites. In another study, Tatibouët[21] analyzed the formation of these products through transient isotopic experiments, concluding that the only possible pathway for the formation of DMM and MF is via hemiacetal. Moreover, this pathway is also supported by DFT calculations[23,26]. Nevertheless, the reason why hemiacetal has not been proposed in precedent FTIR studies is that this intermediate is highly unstable on the surface and therefore cannot be observed in those experiments[27].

In a recent work, Broomhead et al.[24] presented a comprehensive mechanism in which all possible pathways may occur, depending on the structure and availability of the active sites. In this context, they highlighted that MF is more rapidly produced via formaldehyde dimerization pathway or Tishchenko reaction (2 HCHO → $HCOOCH_3$). This pathway had previously been proposed by Mamoru Ai[9,28], who studied it using various mixed oxides and argued that MF may form this way on Lewis's acid sites such titania.

In an effort to dilucidated the reaction mechanism, molybdenum-based catalysts were studied in our recent work[29]. These catalysts exhibit a behavior similar to that described by Broomhead et al.[24] for V_2O_5/TiO_2 catalysts. Catalysts with Mo or V loadings theoretically below the monolayer coverage proposed by Wachs[30] which feature exposed titania, present higher yields to MF, while catalysts that present crystalline molybdenum or vanadium oxides

(above the theoretical monolayer) mainly produce FA or DMM. However, despite these observations, a key uncertainty remains regarding the precise role of titania in MF formation. In particular, it is unclear whether the Tishchenko pathway is truly operative under reaction conditions, or whether an alternative mechanism governs the reaction.

To address this, the present study examines the mechanistic hypotheses discussed above using spectroscopic and isotopic transient experiments under controlled reaction conditions. By correlating structural features with reaction product distribution, the role that titania plays in promoting MF formation is elucidated and the mechanisms proposed in the literature are integrated into a coherent reaction scheme. This integrated approach not only clarifies the surface chemistry involved but also strengthens the correlation between structure and activity, in an effort to deepen the understanding for the selective oxidation reactions over molybdenum catalysts.

Hypothesis and objectives

Hypothesis:

The mechanism of dimethoxymethane (DMM) and methyl formate (MF) formation over MoO_3/TiO_2 and V_2O_5/TiO_2 catalysts proceeds through the hemiacetal pathway, which operates exclusively on sites provided by the metal oxide. In contrast, on Lewis's acid sites associated with titania, MF can be produced via methanol dehydrogenation and oxidation, that is, through the pathway involving formate species as intermediates.

On titania, the formation of methyl formate is more strongly associated with pathways involving formate species generated at metal – titania interfaces, rather than with the Tishchenko – type conversion of formaldehyde occurring exclusively on titania Lewis's acid sites.

General objective:

To study the effect of different types of active sites on the mechanism of the oxidative dehydrogenation of methanol over molybdenum and vanadium catalysts supported on titania.

Specific objectives:

- To propose a reaction mechanism based on the reaction intermediates observed by *in situ* IR spectroscopy.
- To clarify the role of the Lewis acidic sites provided by titania in the formation of methyl formate through the oxidative dehydrogenation of methanol.
- To study the role of hemiacetal as intermediate in the formation of dimethoxymethane and methyl formate.

Chapter I: Deciphering the mechanism of methanol oxidative dehydrogenation on MoO_3/TiO_2 catalysts through Transient and Isotopic Operando-DRIFTS

They say it is better to deal with the devil you know than the one you do not. The molybdenum–based catalysts presented in this thesis were previously synthesized and studied in another investigation carried out within the CarboCat group. That earlier work served as the foundation that inspired a deeper exploration of methanol partial oxidation.

Thus, prior to the start of this chapter, the materials had already been extensively characterized and examined from a surface perspective, which enabled this study to focus on a more detailed understanding of the mechanistic implications associated with the active sites involved. The main goal was to establish a coherent mechanistic picture, integrating key arguments from the different proposed pathways and identifying the most determining factors in this reaction.

This chapter invites the reader to follow that quest. An effort to decipher how the catalyst structure, its active sites, and surface dynamics intertwine to shape the reaction mechanism. It unveils connections that not only deepen the understanding of the role of molybdena but also open new perspectives on the fundamental principles governing the oxidative dehydrogenation of methanol.

I.1. Experimental

I.1.1. Catalysts preparation

MoO_3/TiO_2 supported catalyst with different molybdenum surface density (2.5 and 15 Mo atoms nm^{-2}) were prepared by wet impregnation using ammonium heptamolybdate as precursor and oxalic acid as complexing agent. The desired surface concentration was defined as the number of molybdenum atoms per square nanometer of the catalyst surface, calculated from the nominal MoO_3 weight loading and the BET surface area of the TiO_2 support (50 $m^2\ g^{-1}$, Evonik P–25).

The preparation involved dissolving oxalic acid in water at mild heating, adding the molybdenum precursor to a 3:1 oxalic acid:Mo molar ratio, and subsequently incorporating the support under stirring. After impregnation, the slurry was dried under reduced pressure and then oven–dried, followed by calcination in static air at 500 °C. The same procedure was applied to all catalysts, adjusting only the amount of precursor to reach the desired Mo surface density.

I.1.2 Catalytic activity

Kinetic measurements of the MoO_3/TiO_2 catalysts were performed in a fixed bed reactor. The reactor bed was composed of 200 mg of catalyst mixed with 2 g of quartz sand (both in the range of 150–380 μm particle size), to prevent heat transfer limitations in reaction rate measurements. This mixture was placed between two quartz wool sections.

Before the reaction, the catalyst was pretreated in dry air flow (21 % vol O_2/N_2, Air Liquide, 20 ml min^{-1}) at 300 °C for 30 min at a heating rate of 10 °C min^{-1}. After that, the activity of the catalysts was measured with CH_3OH/O_2 molar ratio equal to 4:9 (P_{CH3OH} = 4 kPa, P_{O2} = 9 kPa, with N_2 as balance) in a total flow of 50 ml min^{-1}. CH_3OH (Merck-Millipore, 99.9%) was fed to the reactor using a PTFE saturator submerged in a thermostatic bath at 25 °C, using N_2 as the bubbling gas. The N_2 (Air Liquide 99.999%) and dry air (Air Liquide 99.999%) flows were controlled by mass flow controllers (Kofloc 8500). The concentration of reagents and reaction products were monitored in real-time using an SRI 8610C gas chromatograph equipped with a capillary column (30 m × 0.53 mm I.D. 1.0U MXT-WAX, Restek 70655-273) and three packed columns (6' × 1/8", Molecular sieve 5A, 18" × 1/8" Hayesep D, and 6' × 1/8" Hayesep D) and an Extorr XT-100 residual gas analyzer. Methanol and reaction product lines were held at 100 °C to prevent condensation.

The selectivity (S_i) for FA, MF and DMM was defined as the outlet molar flow of product i (F_i), multiplied by the number of carbon atoms in that product ($\nu_{C,i}$), normalized by the total contributions of all products, as shown in equation 1.

$$S_i = \frac{\nu_{C,i} \cdot F_i}{\sum_{j=1}^{products} \nu_{C,j} \cdot F_j} \times 100 \quad (1)$$

I.1.3 Operando - Diffuse Reflectance Infrared Fourier Transform Spectroscopy (Operando - DRIFTS)

Operando-DRIFTS analyses were performed using a Praying Mantis system (Harrick Scientific) equipped with a low dead volume stainless-steel cell fitted with ZnSe windows. The temperature of the catalyst in the cell was measured and controlled with a temperature controller (Watlow Instruments) equipped with two K-type thermocouples. The system was located inside a Nicolet iS-20 spectrometer (Thermo Scientific) with a liquid nitrogen-cooled mercury−cadmium−telluride (MCT-A) detector. The respective background spectrum at the corresponding temperature and reactant atmosphere was subtracted. Effluents at the cell outlet were analyzed online using an Extorr XT-100 residual gas analyzer. Gas flows were controlled with mass flow controllers (Kofloc 8500), and a four-way valve allowed for two different reaction systems to be alternately connected to the cell.

Spectra were recorded in the range of 4000 to 400 cm^{-1}, with a sampling frequency of 0.251 s^{-1} and 10 scans per spectrum, and the time-domain IR spectra were recorded in kinetic and

rapid-scan mode at a resolution of 4 cm^{-1}. The feed components for the experiments included N_2 (Air Liquide, 99.999%), dry air (Air Liquide, 99.999%), Ar (Air Liquide, 99.999%), He (Air Liquide, 99.999%), CH_3OH and CD_3OD (both from Merck-Millipore), which were introduced into the feed through a custom-designed glass saturator. Saturation conditions were estimated using the Antoine equation at 25°C. To prevent condensation of methanol and reaction products, all transfer lines were heated and maintained at 100°C.

Two experiments were performed at 175 and 225°C under atmospheric pressure using 2.5 and 15 MoO_3/TiO_2 catalysts. In the first experiment, both systems were subjected to standard reaction conditions (1 kPa CH_3OH, 9 kPa O_2, 10 kPa He as tracer, 10 kPa Ar as internal standard and N_2 as balance). After reaching steady state, the feed was changed to 1 kPa CD_3OD, 9 kPa O_2, 10 kPa Ar, and N_2 as balance (without He). The change was from CH_3OH to CD_3OD and vice versa. The background was collected before methanol entered the cell for the first time.

In the second experiment, first, the system reached steady state under reaction conditions (1 kPa CH_3OH, 9 kPa O_2, 10 kPa He, 10 kPa Ar and N_2 as balance). Then, the feed was changed to (10 kPa Ar and N_2 as balance) to purge the surface and gas phase. After the purge, 1 kPa CD_3OD, 10 kPa Ar, and N_2 as balance were introduced to study the reaction of a deuterated methanol stream with a surface containing hydrogenated species. Subsequently, the feed was switched to 17 kPa O_2, 10 kPa Ar and N_2 as balance to oxidize species formed with CD_3OD. Finally, CH_3OH was reintroduced (1 kPa CH_3OH, 10 kPa Ar, and N_2) in the absence of O_2 to react with D-containing intermediates. Background spectra were collected before each condition. All the experiments were carried out at a total flow rate of 40 ml min^{-1}, and each reaction step was maintained for 30 minutes.

I.2. Results and Discussion

Based on our previous work [27], these catalysts were studied and characterized in our previous work using complementary structural and spectroscopic techniques, revealing a clear dependence of the MoO_3 structures and physicochemical properties on surface molybdenum density[27]. For loadings theoretically below the monolayer coverage (2.5 MoO_3), molybdenum oxide is present as highly dispersed octahedral oligomeric chains strongly interacting with the TiO_2 support. In contrast, above the theoretical monolayer coverage (15 MoO_3), these surface species coexist with, and are largely dominated by, orthorhombic crystalline MoO_3 domains, leading to a partial loss of Mo dispersion and site accessibility. This structural transition entails a shift from highly dispersed, strongly interacting sub monolayer Mo species with high reducibility to bulk crystalline MoO_3 domains characterized by a predominant Mo^{+6} oxidation state, defining two distinct catalytic regimes relevant to methanol activation and selectivity.

Table 1 summarizes the catalytic activity for 2.5 and 15 MoO_3/TiO_2 catalysts in fixed-bed reactor experiments, as reported in our previous publication[27]. Despite operating at comparable methanol conversion (~18%), the two catalysts exhibit markedly different catalytic behavior. The oligomeric catalyst (2.5 MoO_3) presents higher selectivity toward DMM and MF, whereas the crystalline catalyst (15 MoO_3) displays significantly higher activity and a strong preference for FA formation. These results demonstrate that the structural differences between the oligomeric and crystalline MoO_3 phase translate into distinct reactivity and selectivity patterns, consistent with the presence of different surface environments and reaction pathways.

Table 1. Summary of catalytic performance of MoO_3/TiO_2 catalysts of our previous work. Reaction conditions: $CH_3OH/O_2/N_2$ (feed) = 4/9/87 %v/v, T = 225°C, Conversion ca. 18%.

Catalyst	MoO_3 phase	r_{ODH} (μmol s^{-1} g_{cat}^{-1})	S_{FA} (%)	S_{DMM} (%)	S_{MF} (%)
2.5 MoO_3/TiO_2	Octahedral Oligomeric	0.5	19	25	56
15 MoO_3/TiO_2	Orthorhombic Crystalline	2.1	64	11	25

Building on these observations, the following sections explore the behavior of these catalysts under operando-DRIFTS conditions. Figure I–1 displays the evolution of IR bands upon switching the feed from $CH_3OH/N_2/Ar$ (a) and $CD_3OD/N_2/Ar$ (b) to $O_2/N_2/Ar$ at 200 °C, over 2.5 MoO_3 catalyst. In general, the intensity of some bands diminishes under these oxidative conditions, due to the consumption of the respective surface species generated under previous

reaction conditions. Simultaneously, other bands increase in intensity, corresponding to the formation of surface species from the oxidation process.

Figure I–1.a presents the experiment carried out with CH_3OH (H–methanol), where the bands at 2956/2855 cm^{-1} along with those at 2940/2925/2925/1455/1440 cm^{-1}, are associated to molecular methanol species adsorbed on the surface and methoxy species, respectively[17,29]. These bands diminish in intensity under oxidizing conditions due to the consumption of the associated species. Consequently, new bands emerge at 1545/1381/1355 cm^{-1}, which are attributed to adsorbed formates.

Applying the same logic to Fig. I–1.b, the bands observed at 2230/2188/2122/2083/2064 cm^{-1} can be assigned to adsorbed methanol or methoxy species from CD_3OD (D–methanol). Groff[31] studied the adsorption of CD_3OD on molybdenum trioxide on IR and reported that the bands at 2230/2083 cm^{-1} correspond to the asymmetric and symmetric stretching of volatile methanol, respectively. Similarly, the bands at 2185/2064 cm^{-1} were associated with the same vibrational modes in nonvolatile methanol, supporting the hypothesis that these signals arise from adsorbed methanol or methoxy species.

In line with this, Domen et al[32], carried out an IR study following formates species during H_2/D_2 exchange reactions and confirmed that all the bands emerging under oxidizing conditions in our experiments (2203/1525/1327 cm^{-1}) correspond to formates. The 2203 cm^{-1} band is a shifted counterpart of the 2940 cm^{-1} band, associated with formates (ν_{as} (CO_2) + δ(C-H))[33]. Meanwhile, the bands at 1525 and 1327 cm^{-1} correspond to slightly shifted from the 1545 and 1381 cm^{-1} bands observed in the hydrogenated case. In Fig. I–1.b, the 1525 cm^{-1} band appears poorly defined and close with the 1545 cm^{-1} band, while the 1327 cm^{-1} band is more distinct and clearly separated from the 1381 cm^{-1} band. For this reason, these species (hydrogenated or deuterated) will be followed in all subsequent experiments. Furthermore, these bands were also detectable on the 15 MoO_3 catalyst (Figure I–2).

In both transitions $CH_3OH/N_2/Ar$ to $O_2/N_2/Ar$ (with H- and D-methanol), a negative peak is observed at 1612 cm^{-1}, corresponding to the δ(H–O–H) modes of strongly Lewis – bound water on the catalyst. The appearance of this negative feature after methanol adsorption and oxidation indicates that methanol adsorption displaces the Lewis-bound water[34,35].

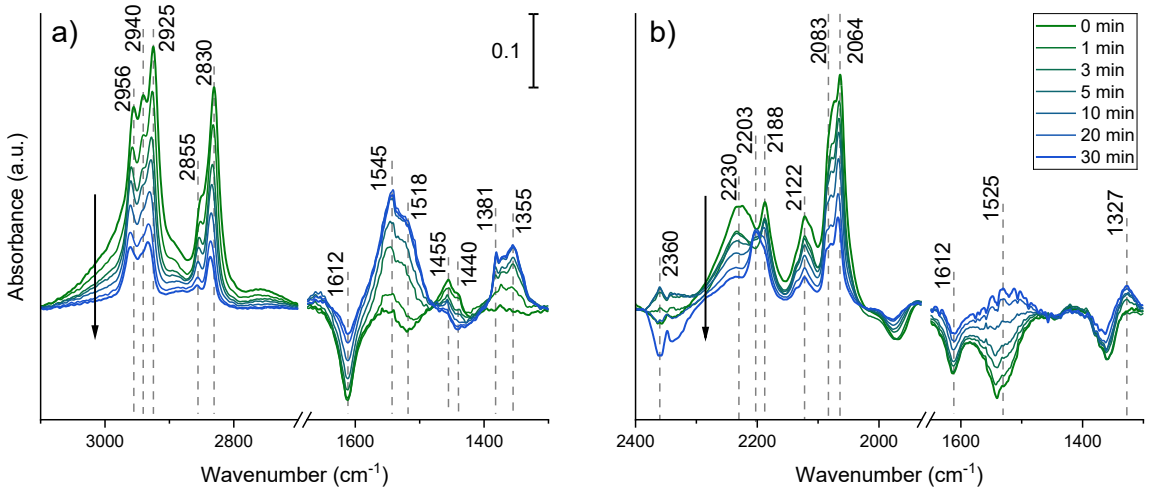

Figure I–1 DRIFT spectra of 2.5 MoO_3/TiO_2 catalyst at 200°C after switching from a) $CH_3OH/O_2/N_2/Ar$ to $O_2/N_2/Ar$; b) $CD_3OD/O_2/N_2/Ar$ to $O_2/N_2/Ar$.

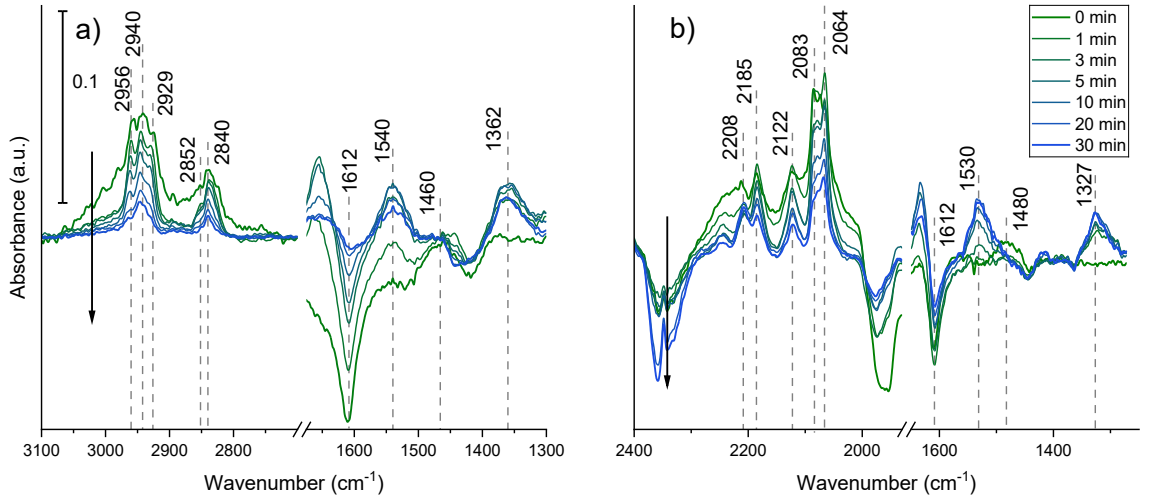

Figure I–2 DRIFT spectra of 15 MoO_3/TiO_2 catalyst at 200°C after switching from a) $CH_3OH/O_2/N_2/Ar$ to $O_2/N_2/Ar$; b) $CD_3OD/O_2/N_2/Ar$ to $O_2/N_2/Ar$.

Figure I–3 shows the transient experiments at 225°C where the feed was switched between $CH_3OH/O_2/N_2/Ar/He$ and $CD_3OD/O_2/N_2/Ar$, over both Mo–Ti catalysts, focusing on the formation of methyl formate. During the H → D transition (Fig. I–3 a and c), after helium evacuation, the signal of fully hydrogenated methyl formate ($HCOOCH_3$) also decreases at a similar rate in both catalysts. A few seconds later, the main product of this transition appears, methyl formate with a fully deuterated methoxy group ($HCOOCD_3$). The temporal evolution of the $HCOOCD_3$ signal reveals differences in the kinetic behavior of both catalysts. The broader and longer–lasting peak observed for 2.5 MoO_3 suggests slower reaction kinetics and higher selectivity, while the narrower profile of the same product over 15 MoO_3 indicates a more active catalyst with lower selectivity toward MF. At the end of the

transition, fully deuterated methyl formate ($DCOOCD_3$) appears. Notably, the formation rates (slopes) of $DCOOCD_3$ differ between catalysts, which may again be related to their activity in the context of isotopic effects.

To rationalize these transient behaviors, Scheme I–1 summarizes the reaction pathways most commonly proposed in the literature for methanol oxidation and MF formation[12,15,16,24], as discussed above in the introduction. Scheme I–1.a outlines the general mechanism of oxidative dehydrogenation of methanol, while Scheme I–1.b highlights the incorporation of CD_3OD in each pathway. This compiled scheme provides the framework needed to interpret the isotopologue sequence observed in Figure I–3.

The sequence of formation of methyl formate isotopologues observed during this transition is consistent with the Scheme I–1. If the reaction proceeds via either formate species (HCOO) route or the hemiacetal intermediate (CH_3OCH_2OH), feeding CD_3OD results in the interaction of deuterated alcohol with hydrogenated surface intermediates, coming from formaldehyde (HCHO) such as hemiacetal or formate. In either case, the only MF isotopologue possible during this transition is $HCOOCD_3$ and once the hydrogenated surface intermediates are consumed, the sole product formed is $DCOOCD_3$.

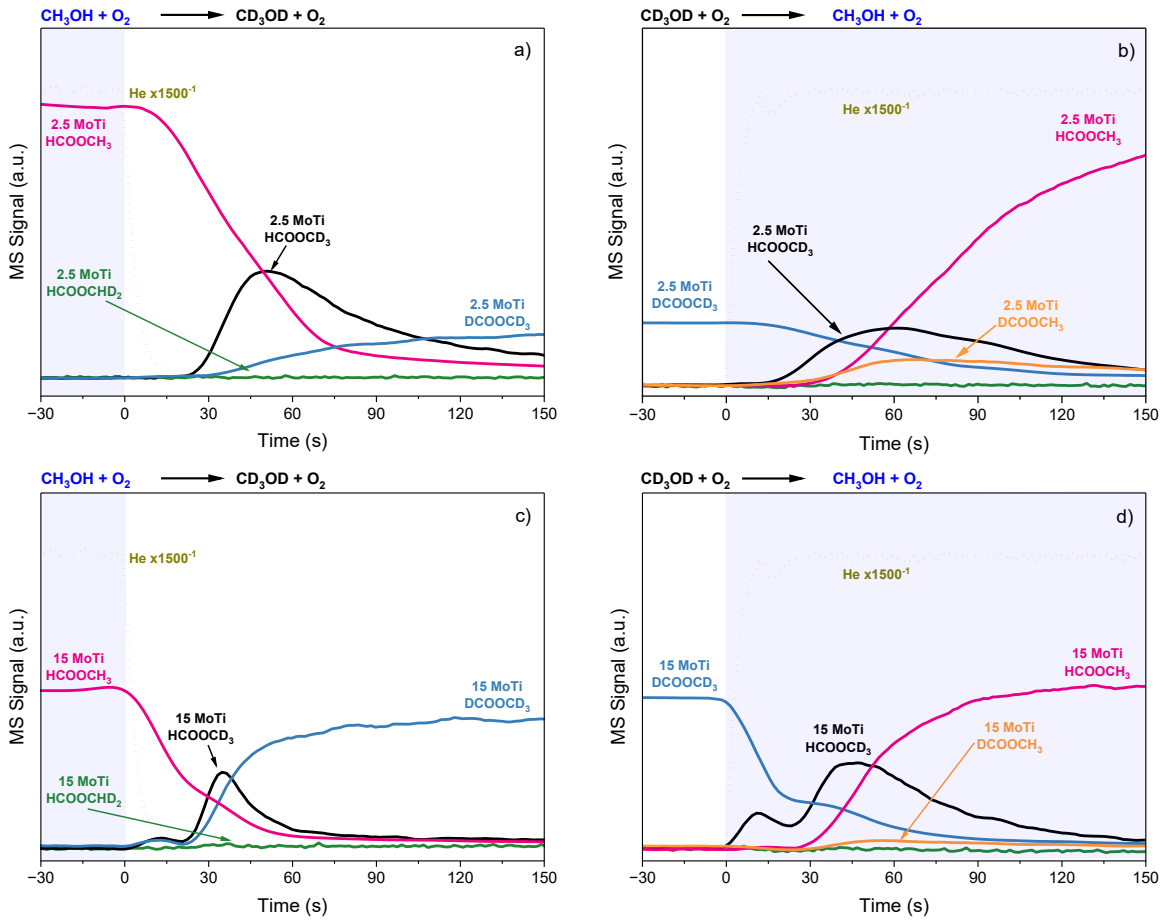

Figure I–3 MS signal of methyl formate (hydrogenated, partially, and fully deuterated) in the $CH_3OH/O_2/N_2/Ar/He \rightarrow CD_3OD/O_2/N_2/Ar$ or vice versa transition at 225°C for a) 2.5 MoO_3 catalyst $CH_3OH \rightarrow CD_3OD$; b) 2.5 MoO_3 catalyst $CD_3OD \rightarrow CH_3OH$; c) 15 MoO_3 catalyst $CH_3OH \rightarrow CD_3OD$; d) 15 MoO_3 catalyst $CD_3OD \rightarrow CH_3OH$.

Applying the same logic, during the D → H transition, the expected main product would be $DCOOCH_3$. However, this species is detected after the apparition of $HCOOCD_3$ or even H-MF ($HCOOCH_3$), these compounds appear earlier and in greater proportion than $DCOOCH_3$ (Fig. I–3.b and I–2.d). This is an intriguing result: while the formation of $HCOOCD_3$ during H → D transition is consistent with the formate or hemiacetal pathway, its predominance during the D → H transition is unexpected and suggests the influence of an additional effect. A kinetic isotope effect could contribute to this behavior, since the conversion levels differ under H- and D-methanol feeds, and may help explain why the formation of $HCOOCD_3$ is notoriously greater compared to $DCOOCH_3$.

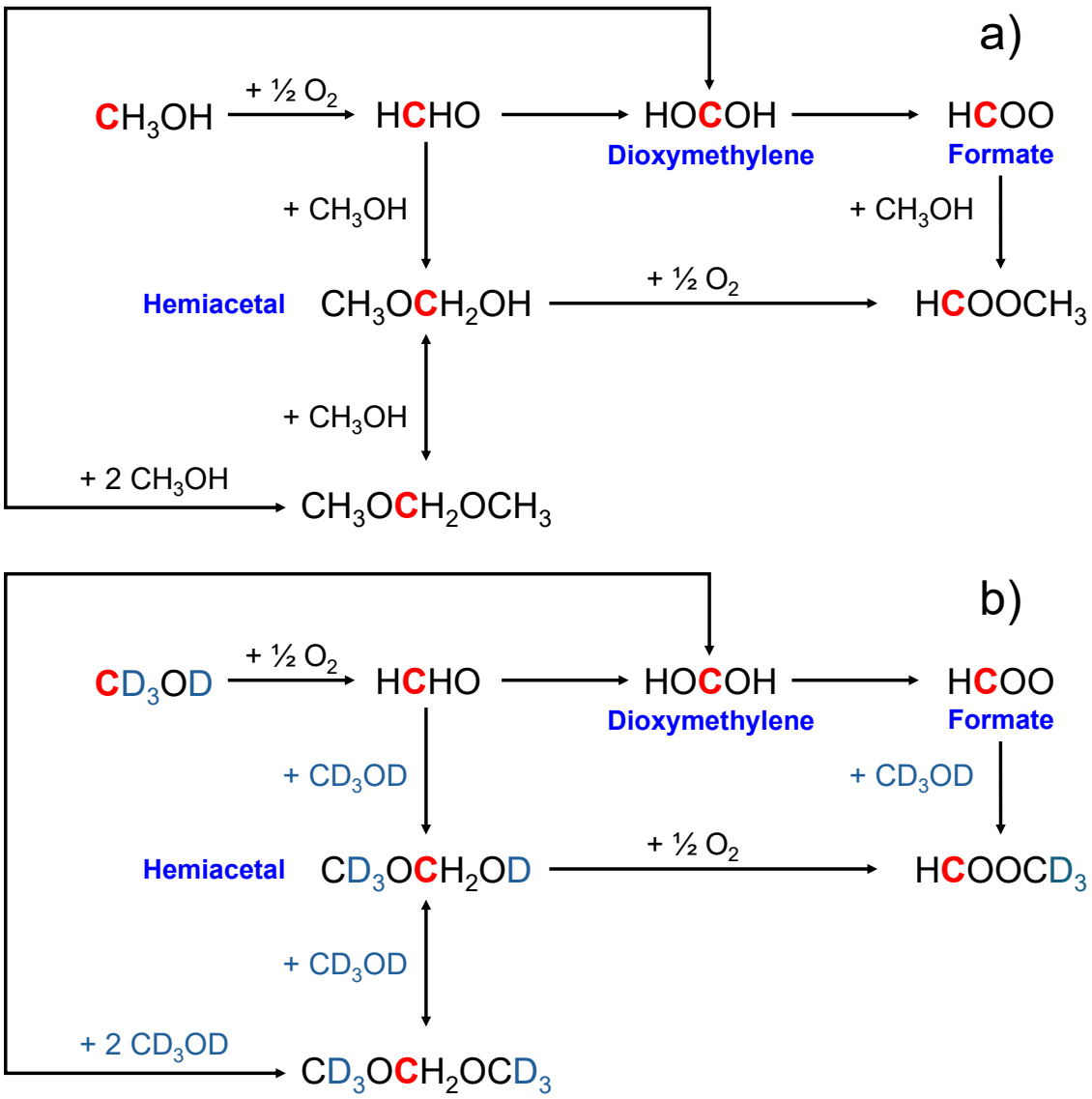

Scheme I–1 Surface dioxymethylene – formate and hemiacetal intermediate pathways proposed for the methanol ODH reaction, considering a) the fully hydrogenated case, and b) hydrogenated intermediates with deuterated methanol in the gas phase.

It is worth noting that the Tishchenko reaction pathway does not account for the above observation. In both transitions, MF with a partially deuterated methoxy group ($HCOOCHD_2$) was not detected. This compound would be expected if the formation of MF occurred via Tishchenko reaction, which involves the reaction of hydrogenated and deuterated formaldehyde (HCHO + DCDO). This scenario is theoretically possible, Cant et al.[36], reported that when CH_3OH and CD_3OH were co-fed during the non-oxidative dehydrogenation of methanol over copper – based catalysts, small amounts of $HCOOCHD_2$

were observed. Nevertheless, the main product reported in their study was $HCOOCD_3$, which is consistent with our findings.

Broomhead et al.[24] reported that MF is formed via the Tishchenko reaction over V_2O_5/TiO_2 catalysts with exposed titania based in their characterization. Isotopic labeling experiments, using CD_3OD and HCHO or the other way (CH_3OH and DCDO), showed that once MF is generated through the Tishchenko pathway, an exchange takes place between the methoxy groups (CH_3O*) from methanol and those of methyl formate. This isotopic exchange is exemplified by the following reaction: $CD_3OD + HCOOCH_3 \rightleftarrows CH_3OD + HCOOCD_3$. Nonetheless, Takahashi et al.[37], provided more definitive evidence against this mechanism in their study over Cu/SiO_2 catalyst in the non-oxidative dehydrogenation of methanol. They co-fed H-FA (HCHO) and D_3-methanol (CD_3OH) at temperatures where Tishchenko reaction typically occurs, and the predominant product was $HCOOCD_3$. Importantly, they did not detect methanol produced by methoxy exchange between H-MF and deuterated methanol. In fact, they reported that methyl exchange occurred in less than 2%, rendering it insignificant. Moreover, rearranging hydrogen or deuterium atoms within the methoxy group is also unlikely, as this would require breaking a C-H (or C-D) bond, a step known to be the RDS in methanol oxidation.

In line with the findings of Cant[36], Takahashi et al.[37] further showed that when co-feeding CH_3OH and CD_3OH, the formation rates of $HCOOCH_3$ and $HCOOCD_3$ species were three to five times higher than those of $DCOOCH_3$ and $DCOOCD_3$. Pearson et al.[38] also reported similar results. Taking together, these studies and our own results indicate that $HCOOCD_3$ formation is favored, even in conditions where $DCOOCH_3$ would theoretically be accessible. This preferential formation reflects the fact that hydrogen abstraction during methanol dehydrogenation is kinetically more favorable than deuterium abstraction, leading to substantially higher rates of pathways involving HCHO than those involving DCDO.

Figure I–4 summarizes the $CH_3OH/O_2/N_2/Ar/He \rightarrow CD_3OD/O_2/N_2/Ar \rightarrow CH_3OH/O_2/N_2/Ar/He$ transition for the 2.5 MoO_3 catalyst at 175°C. Fig. I–4.a shows the evolution of fully hydrogenated or deuterated MF and DMM throughout the experiment, while Fig. I–4.b and I–4.c provide magnified views of the transitions where the feed composition was switched. At this temperature, both DMM and MF decay at nearly the same rate under deuterated conditions, indicating that they share the same rate-determining step, i.e., the first dehydrogenation of the methoxy group. Since they decay in the same proportion, it can be concluded that only one methanol species is involved in the RDS.

Complementary data at 225°C for the same catalyst, and for 15 MoO_3 at both 175 and 225°C are presented in Figure A.I–1 – A.I–3 respectively. Under deuterated reaction conditions, the reaction is slightly shifted toward the formation of fully deuterated DMM (D-DMM). This shift reflects the equilibrium between DMM and its surface precursor, which depends on

reaction conditions and the H_2O pressure. At higher activity, this intermediate tends to participate in the pathways leading to MF [12,18,29]. In the case shown in Fig. I–4, the reaction operates in kinetic regime, where equilibrium limitations are negligible and the formations of DMM or MF are not thermodynamically favored.

Therefore, the fact that both DMM and MF decay in the same proportion, and that no equilibrium effects favoring DMM formation are observed, indicates that both products share the same RDS. Assuming that the first dehydrogenation of methanol is the RDS [12,16,39], the kinetics do not allow the Tishchenko reaction pathway to operate as the mechanism for the methyl formate formation, as it would result in a more pronounced decrease under deuterated conditions compared to DMM. This is because, if MF were formed through the Tishchenko mechanism, the amount of FA required would be twice that needed for DMM formation.

During the methanol transition, DMM is the first product to disappear (Fig. I–4.b and I–4.c and all the Fig. A mentioned recently). This behavior is probably related to the last methanol molecules participating in its formation, which may remain in the gas phase rather than as surface methoxy species. If this assumption is correct, it implies that methoxy species can follow two different pathways on the surface: (I) dehydrogenation to formaldehyde, or (II) direct participation in the formation of MF. Considering the previously discussed kinetic isotope effect during $CD_3OD \rightarrow CH_3OH$ transition, it is reasonable to assume that deuterated methoxy species accumulate on the catalyst surface due to the slower rate-determining step, resulting in higher surface coverage. As a result, when H-methanol reaches an available redox site, and considering that H-methanol is dehydrogenated to formaldehyde more readily than D-methanol, it facilitates the removal of surface deuterated intermediates. This provides a consistent explanation for why $HCOOCD_3$ becomes the dominant product during the $CD_3OD \rightarrow CH_3OH$ transition.

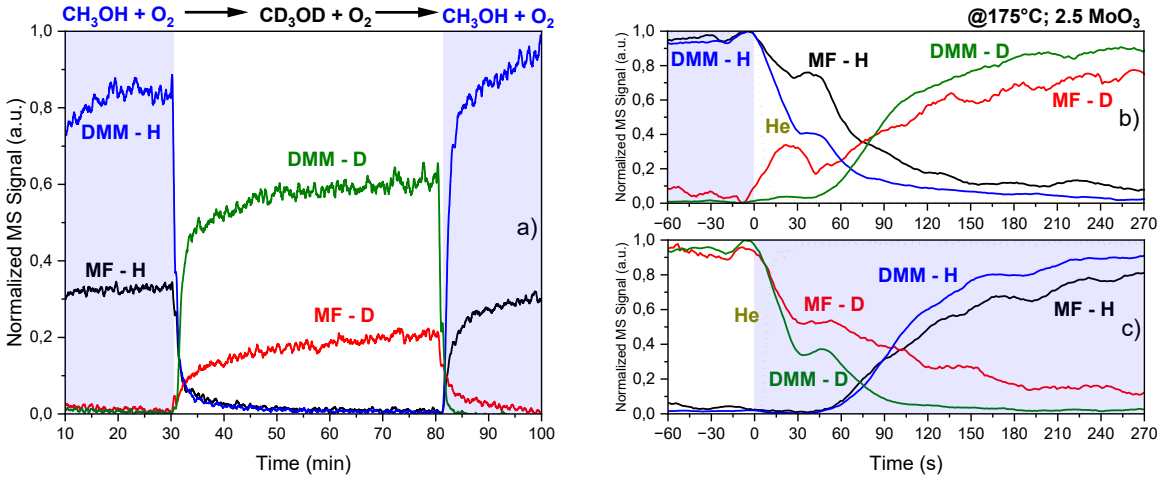

Figure I–4 Normalized MS signal of methyl formate (MF) and dimethoxymethane (DMM), fully hydrogenated (H) and deuterated (D), a) $CH_3OH/O_2/N_2/Ar/He \rightarrow CD_3OD/O_2/N_2/Ar \rightarrow CH_3OH/O_2/N_2/Ar/He$ transition over 2.5 MoO_3/TiO_2 catalyst at 175°C, b) zoom of $CH_3OH \rightarrow CD_3OD$ transition and c) zoom of $CD_3OD \rightarrow CH_3OH$ transition

As shown in Figure I–5, the IR signals corresponding to hydrogenated (2925 cm^{-1}) and deuterated (2064 cm^{-1}) methoxy groups, together with transient evolution of the MF isotopologues during $CH_3OH \rightarrow CD_3OD$ transition, exhibit nearly identical profiles over both catalysts. The parallel evolution of the 2925 cm^{-1} band and fully hydrogenated methyl formate further indicates that the decrease in $HCOOCH_3$ is related to the consumption of surface methoxy species, either through dehydrogenation to formaldehyde or direct involvement in MF formation, this is consistent with the previously pathways and does not support their participation in a Tishchenko-type mechanism.

If the Tishchenko pathway were the main pathway, an exchange between the methoxy group of $HCOOCH_3$ and the deuterated methoxy of CD_3OD would lead to different evolution profiles. Specifically, the consumption of CH_3O^* should lag the formation of CD_3O^*, and $HCOOCD_3$ should appear earlier than CD_3O^*. Furthermore, the distinct slopes of the $HCOOCD_3$ signal compared to other species suggest that CD_3OD reacts with a surface enriched in hydrogenated species coming from HCHO, ultimately yielding the partially deuterated compound.

On the other hand, the potential methoxy exchange was rigorously examined in Appendix AI–2. A quantitative analysis of the accumulation of hydrogenated and deuterated methoxy species during the formation of $HCOOCD_3$ in the transient experiments indicates that such an exchange does not take place. This independent evaluation reinforces that the isotopic profiles observed here cannot be attributed to a methoxy – methoxy scrambling mechanism.

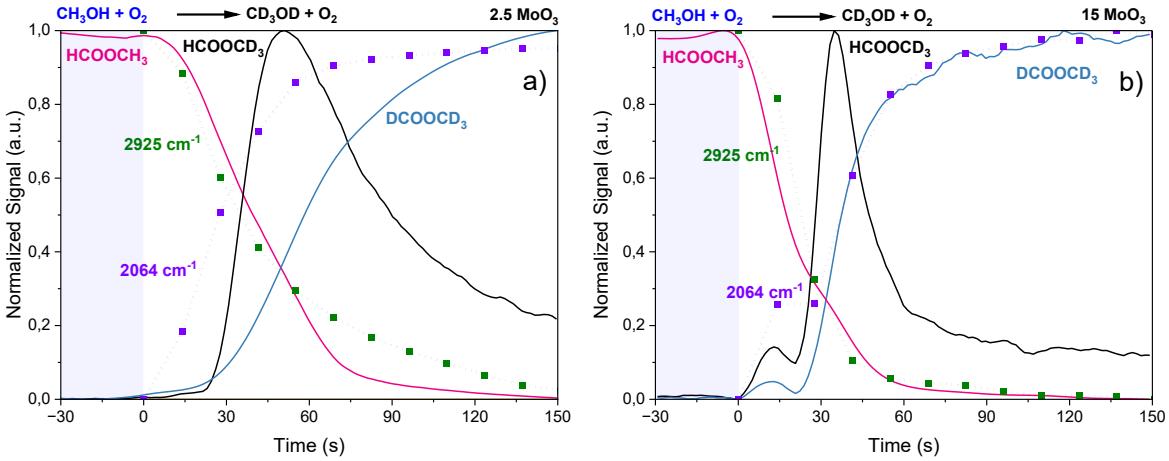

Figure I–5 Normalized MS signal of methyl formate (hydrogenated, partially, and fully

deuterated) in the $CH_3OH \rightarrow CD_3OD$ transition at 225°C and methoxy hydrogenated (2925 cm^{-1}) and fully deuterated (2064 cm^{-1}) normalized IR evolution on a) 2.5 MoO_3 catalyst; b) 15 MoO_3 catalyst.

Figure I–6 shows the IR spectra during $CH_3OH/O_2/N_2/Ar/He \rightarrow CD_3OD/O_2/N_2/Ar$ (a) and $CD_3OD/O_2/N_2/Ar \rightarrow CH_3OH/O_2/N_2/Ar/He$ (b) transition over the 2.5 MoO_3 catalyst, within the first two minutes after the switch. The green spectra correspond to the steady-state condition before the change, while the blue spectra were collected 2 minutes after the switch. The Figure highlights three spectral regions: hydrogenated methoxy (2800 – 3000 cm^{-1}), deuterated methoxy (2000 – 2300 cm^{-1}) and formates (1300 – 1600 cm^{-1}). In both transitions, the evolution of H- and D-methoxy bands is remarkably clean. However, formate species were not observed on the catalyst surface under any condition. This behavior was consistent for both catalysts (2.5 and 15 MoO_3 catalyst) at 175 and 225°C. Nevertheless, this result does not discard that the formates participate in the formation of MF. It is probable that the surface formates have a short-life time or are not formed in detectable amounts.

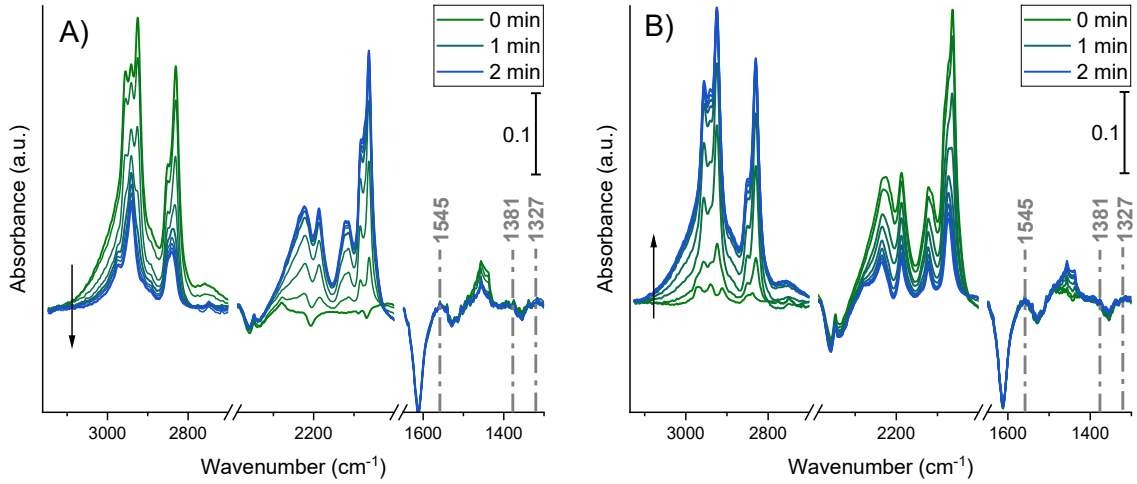

Figure I–6 IR spectra for 2.5 MoO_3/TiO_2 catalyst at 225°C during a) $CH_3OH/O_2/N_2/Ar/He \rightarrow CD_3OD/O_2/N_2/Ar$ transition; b) $CD_3OD/O_2/N_2/Ar \rightarrow CH_3OH/O_2/N_2/Ar/He$ transition.

Summarizing the results of these experiments, the Tishchenko reaction can be ruled out for MoO_3/TiO_2 catalysts, and it remains unclear whether formates participate in the formation of MF. Moreover, the formate and hemiacetal pathways lead to the same deuteration pattern in MF, resulting in $HCOOCD_3$. The slower formation of $DCOOCH_3$ compared to $HCOOCD_3$ lies in the kinetic isotope effect operating during the first and second dehydrogenation steps of methoxy group, both associated with the redox site. Furthermore, it remains to be clarified the role titania plays in the selectivity of MF on the 2.5 MoO_3/TiO_2 catalyst.

Figures I–7 and I–8 present complementary views of the transient responses at 225°C for the 2.5 MoO_3 catalysts during $CH_3OH + O_2 \rightarrow N_2 \rightarrow CD_3OD \rightarrow O_2 \rightarrow CH_3OH$ sequence. While

Fig. I–7 displays the gas–phase evolution of MF and its isotopologues for each individual transition, Fig. I–8 provides the continuous IR history of surface intermediates throughout the experiment, each panel showing each individual step (Fig 6.b, c, d and e). The main changes are observed in the first minutes of each panel. During the $CH_3OH + O_2 \rightarrow N_2$ step (Fig. I–7.a), the $HCOOCH_3$ signal in the gas phase decreases upon replacing $CH_3OH + O_2$ with N_2, in line with the simultaneous consumption of H-methoxy surfaces bands (2830, 2925 and 2940 cm^{-1}, Fig. I–8.a and b). While the H-methoxy species are consumed, H-formate-related bands (1381 and 1550 cm^{-1}) rise on the surface during the purge step. When the feed is switched to CD_3OD (Fig. I–7.b), the $HCOOCD_3$ signal appeared in the gas phase together with the gradual formation of $DCOOCD_3$, while in Fig. I–8.c shows the consumption of H-formates species formed in the previous step, accompanied by the increase of D-methoxy species bands (2064, 2122, 2188 and 2230 cm^{-1}). In Fig. I–7.c, corresponding to the $CD_3OD \rightarrow O_2$ step, $DCOOCD_3$ reaches a maximum in its production and subsequently decreases due to the absence of CD_3OD in the feed. In parallel and similar to what is observed in the purge step, Fig. I–8.c and I–8.d, shows the consumption of D-methoxy bands together with growth of D-formates related bands (1327 and 1525 cm^{-1}) under oxidation conditions. Finally, during the last step of this experiment, the switch from O_2 to CH_3OH (Fig. I–7.d), $DCOOCH_3$ is observed as the predominant product, reaching a maximum before decreasing, while in parallel, $HCOOCH_3$ forms steadily throughout the step. Correspondingly, Fig. I–8.e shows the decline of D-formates species while the H-methoxy raise.

The behavior observed in the $N_2 \rightarrow CD_3OD$ step (Fig. I–7.b) is essentially the same as during the $CH_3OH \rightarrow CD_3OD$ transition (Fig. I–3.a): following the decrease of $HCOOCH_3$, the isotopologues of MF appear in the sequence $HCOOCD_3$ and then $DCOOCD_3$. The main difference, however, is that during the $CH_3OH + O_2 \rightarrow N_2 \rightarrow CD_3OD$ transition, surface formates are clearly detected, and once upon CD_3OD is introduced in the cell, the formate-related bands (1381 and 1550 cm^{-1}) are consumed.

Otherwise, during $O_2 \rightarrow CH_3OH$ step (Fig. I–7.d), a markedly different behavior is observed compared to the $CD_3OD \rightarrow CH_3OH$ sequence (Fig. I–3.b), since in this case $DCOOCH_3$ is detected predominantly, rather than $HCOOCD_3$ or $HCOOCH_3$. The main reason is that during $CD_3OD \rightarrow CH_3OH$ transition, the surface becomes saturated with D-methoxy species due to the kinetic isotope effect discussed previously. Under these conditions, any DCOO* species that could be formed would either have a short lifetime or exist in very low amounts on the surface. In contrast, during $CD_3OD \rightarrow O_2 \rightarrow CH_3OH$ sequence, the formation of DCOO* becomes possible because the CD_3OD (CD_3O*) is extensively oxidized to DCOO*. This intermediate is sufficiently stable to remain on the surface and is only consumed upon the subsequent introduction of CH_3OH.

From the above discussion, it is reasonable to conclude that the 2.5 MoO_3 catalyst can both generate and stabilize surface formates, which then act as intermediates in the formation of MF via formate pathway. This interpretation is further supported by Figures I–8.d and I–8.e, which exhibit a similar behavior under comparable conditions for CH_3OH and DCOO*.

In line with the above, an important observation arises from the comparison between Fig. I–7.b and 7.d. Although the products differ due to the use of CD_3OD vs CH_3OH, their overall behavior is similar. This suggests that, under both previous conditions (purge and oxidation step, respectively), the catalyst surface was already saturated with formate species. Consistently, in the previous experiment at 225°C with the 2.5 MoO_3 catalyst (Fig. A. I–1), during the CD_3OD → CH_3OH transition, the alcohol-rich environment (together with the kinetic isotope effect) favored the formation of DMM over MF. This implies that the formation of DCDO and its subsequent conversion to formates is slower than the formation of the formaldehyde – methanol complex leading to DMM. Therefore, in the absence of methanol in the gas phase during CD_3OD → O_2 → CH_3OH transition, DCDO proceeds to form DCOO* until surface methoxy groups are depleted. As a consequence, DMM formation starts from zero, since not partially deuterated DMM molecules are detected, only fully hydrogenated or fully deuterated ones even 175°C (Figure A.I–4). Any mixed isotopologues that might form are only detected after the accumulation of fully H- or D-DMM and can thus be considered irrelevant in the mechanism.

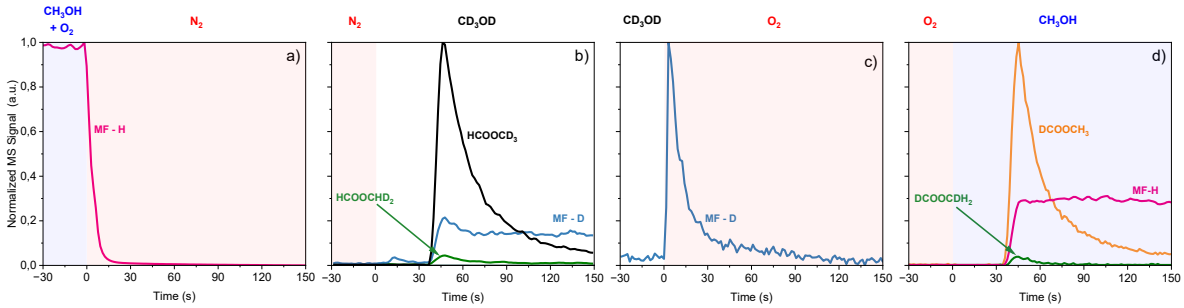

Figure I–7 Normalized MS signal for hydrogenated methyl formate ($HCOOCH_3$, H-MF) and its partially ($HCOOCD_3$; $DCOOCH_3$) and fully deuterated ($DCOOCD_3$, D-MF) homologues during the transition a) $CH_3OH + O_2 \rightarrow N_2$; b) $N_2 \rightarrow CD_3OD$; c) $CD_3OD \rightarrow O_2$; d) $O_2 \rightarrow CH_3OH$ at 225°C for the 2.5 MoO_3 catalyst.

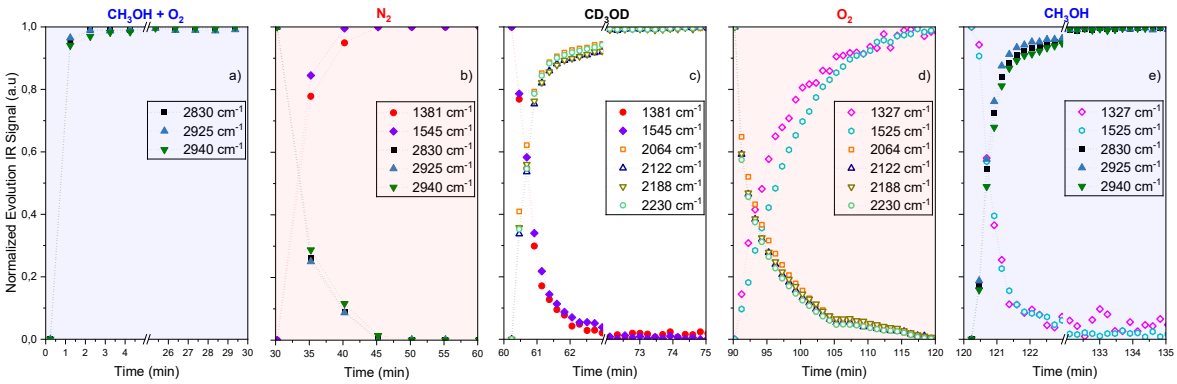

Figure I–8 Normalized IR signal of the evolution of the different intermediates on the surface (H-methoxy bands: 2830, 2925 and 2940 cm^{-1}; H-formate bands: 1381 and 1545 cm^{-1} ; D-methoxy bands: 2064, 2122, 2188 and 2230 cm^{-1} ; D-formate bands: 1327 and 1525 cm^{-1}) of the 2.5 MoO_3 catalyst at 225 °C during each step: a) $CH_3OH + O_2$; b) N_2; c) CD_3OD; d) O_2; e) CH_3OH.

Figures I–9 and I–10 illustrate complementary views of the $CH_3OH + O_2 \rightarrow N_2 \rightarrow CD_3OD \rightarrow O_2 \rightarrow CH_3OH$ sequence for the 15 MoO_3 catalyst at 225°C. As in the case of the 2.5 MoO_3 catalyst, Fig. I–9 corresponds to the gas – phase evolution of MF and its isotopologues, while Fig. I–10 shows the surface intermediates throughout the experiment.

Overall, the transient behavior resembles that observed for 2.5 MoO_3 (Fig. I–7 and I–8). However, the main distinction is that for 15 MoO_3 the products are dominated, during the key transitions (Fig. I–9.b and d), by either fully hydrogenated or deuterated MF. $HCOOCD_3$ and $DCOOCH_3$ are detected in much lower proportions, becoming detectable after the apparition of HCOOCH3 or $DCOOCD_3$. Likewise, Fig. I–10.b and d reveal that, in contrast to 2.5 MoO_3, no detectable HCOO* or DCOO* accumulate on the catalyst surface when methoxy species are consumed during the purge or oxidation step. Aside from these differences, the behavior of $HCOOCH_3$ and $DCOOCD_3$ (Fig. I–9), together with the depletion and reformation of H- and D- methoxy surface species (Fig. I–10), follows the same trends observed in Fig. I–7 and I–8, remaining consistent with the reintroduction of methanol into the feed.

The explanation of the behavior described above lies in the different ability of the 15 MoO_3 catalyst to generate and stabilize surface formates comparing 2.5 MoO_3. As shown in Fig. I–10.b and d methoxy species were consumed without forming detectable formates on the 15 sample, whereas in the case of 2.5 MoO_3 (Fig. I–8.b and d) formates were observed. These methoxy species should be consumed to produce HCHO, consistent with the high selectivity of this catalyst toward that product. Consequently, during the purge and oxidation steps, the surface was effectively cleaned from adsorbed species. As a result, when CD_3OD or CH_3OH was subsequently fed, the reaction starts form a clean surface, producing MF from scratch.

This outcome is not biased by temperature. Figure A.I–5 shows the $CH_3OH + O_2 \rightarrow N_2 \rightarrow CD_3OD$ transition for both 2.5 and 15 MoO_3 catalyst at 175°C. It can be seen that the maximum MF formation occurs at different moments feed compositions. For the 2.5 MoO_3 catalyst, the maximum corresponds to $HCOOCD_3$ during the CD_3OD feed step, whereas for 15 MoO_3, the maximum appears during the reaction stage associated with $HCOOCH_3$. It is worth noting that in the latter catalyst $HCOOCD_3$ is also detected at 175°C, although in significantly lower amounts. This observation is consistent with the presence of surface formates evidenced in Fig. I–2; however, their quantity is expected to be minimal given the highly crystalline nature of the catalyst. Therefore, these findings also demonstrate that the main intermediate leading to MF are inherently unstable on the surface of 15 MoO_3 and differs from that on 2.5 MoO_3.

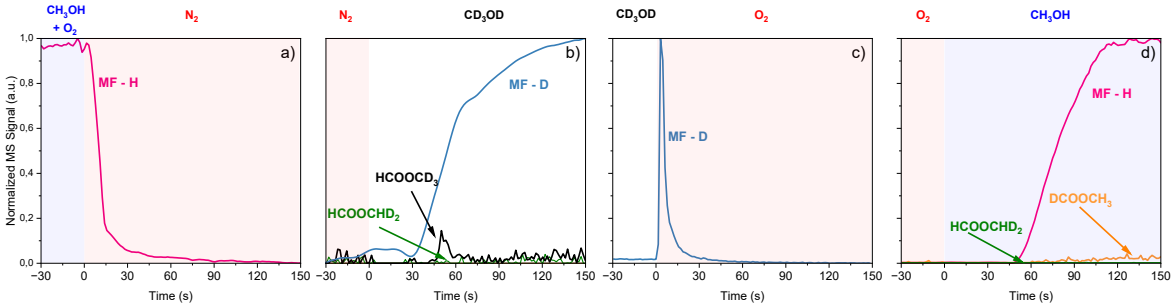

Figure I–9 Normalized MS signal for hydrogenated methyl formate ($HCOOCH_3$, H-MF) and its partially ($HCOOCD_3$; $DCOOCH_3$) and fully deuterated ($DCOOCD_3$, D-MF) homologues during the transition a) $CH_3OH + O_2 \rightarrow N_2$; b) $N_2 \rightarrow CD_3OD$ c) $CD_3OD \rightarrow O_2$; d) $O_2 \rightarrow CH_3OH$ at 225°C for the 15 MoO_3 catalyst.

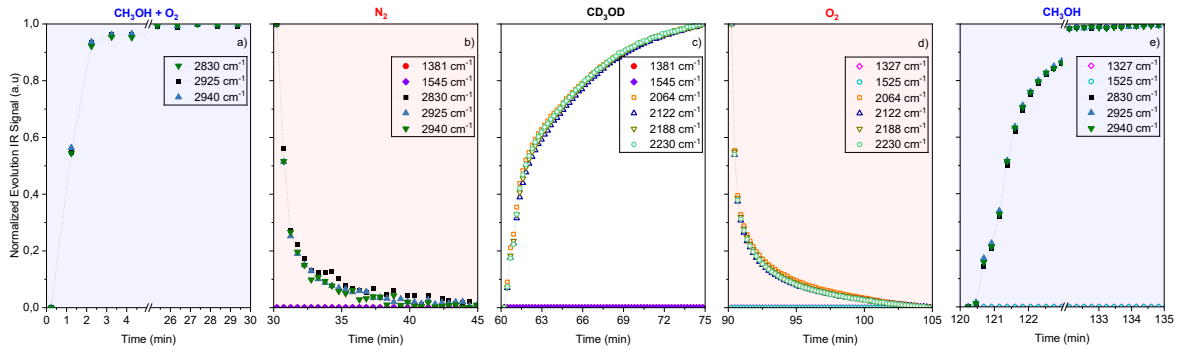

Figure I–10 Normalized IR signal of the evolution of the different intermediates on the surface (H-methoxy bands: 2830, 2925 and 2940 cm^{-1}; H-formates bands: 1381 and 1550 cm^{-1} ; D-methoxy bands: 2064, 2122, 2188 and 2230 cm^{-1} ; D-formate bands: 1327 and 1525 cm^{-1}) of the 15 MoO_3 catalyst at 225 °C during each step: a) $CH_3OH + O_2$; b) N_2; c) CD_3OD; d) O_2; e) CH_3OH.

Recapitulating, the oxidative dehydrogenation of methanol was studied on two catalysts with clearly different structures[29]. The experimental evidence indicated that the predominant methyl formate pathway on the crystalline catalyst with large domain size (15 atoms Mo/nm^2) is related to the hemiacetal route. This is supported by the formation of a partially deuterated product ($HCOOCD_3$) during the $CH_3OH \rightarrow CD_3OD$ transition, which is associated with this mechanism. A second piece of evidence comes from the $CH_3OH + O_2 \rightarrow N_2$ transition, where, after the surface purge with N_2, no methoxy or formate species were detected. When CD_3OD was subsequently introduced, the reaction started from zero. This suggests that the catalyst neither strongly adsorbs intermediates nor stabilizes them over time. Such behavior is consistent with the hemiacetal intermediate, which is known to be unstable[27]. It is worth noting that this catalyst is highly selective toward formaldehyde, likely due to the facilitated desorption promoted by the proximity of its Mo-O-Mo active sites[40].

In contrast, the catalyst with a smaller domain size (2.5 atoms Mo/nm^2), which presents an oligomeric molybdenum structure along with exposed titania[29], also shows the formation of $HCOOCD_3$ during the $CH_3OH \rightarrow CD_3OD$ transition. Moreover, during the $CH_3OH + O_2 \rightarrow N_2$ transition, the surface becomes filled with active formates that effectively participate in the formation of MF.

Does this evidence rule out the hemiacetal pathway for 2.5 MoO_3 catalyst? Not necessarily. Titania alone cannot perform oxidative dehydrogenation[29]; the presence of another metal with a higher redox capacity, such as molybdenum or vanadium, is required. When molybdenum is supported on titania, in addition to redox sites, Brønsted acid sites are also introduced[41], and it is on these acidic sites that the hemiacetal intermediate can form[12,24,25,27,29,39]. Therefore, based on these observations and statements, both mechanisms appear to be plausible.

First of all, during all $CH_3OH + O_2 \rightarrow N_2 \rightarrow CD_3OD \rightarrow O_2 \rightarrow CH_3OH$ transitions, it was observed that the surface intermediates (methoxy and formates species) are stable during all the experiment on 2.5 MoO_3 catalyst, and more notably during the purge or oxidation process at 225°C. On the other hand, this catalyst is not as selective to formaldehyde as DMM or MF. Therefore, it is possible to assume that the role of titanium oxide in this catalyst is to stabilize the intermediates on the surface, starting with formaldehyde.

So, how is the FA adsorbed on the surface? According to studies that investigated the adsorption of formaldehyde using IR spectroscopy, its most stable adsorbed form is dioxymethylene[17,42,43]. Busca[17] indicates that formaldehyde adsorbs on ionic metal oxides, as well as on titania, mostly in the form of dioxymethylene species. It is also reported that on unsupported vanadium surface, when formaldehyde is adsorbed and the temperature raised from room temperature, the detected dioxymethylene species desorb. However, when the

surface is vanadium – titania, dioxymethylene undergoes dehydrogenation to form adsorbed formate species. This behavior could also be consistent with that observed on 2.5 MoO_3/TiO_2 catalysts, suggesting that a similar pathway may operate under the studied conditions.

This raises the question: is this effect solely due to titania, or is it result of a combined interaction between titanium and oligomeric molybdenum? As mentioned above, this reaction does not occur over titania alone. Although molybdenum oxide is known for its high formaldehyde yield, it alone cannot account for the site where the dioxymethylene – formate pathway takes place.

Wachs et al.[10,44], reported that, at interfacial sites on the oxide metallic catalysts, the specific catalytic activity on different oxide supports does not stem from a structural effect, monomer vs polymer, but rather from a ligand effect imposed by the different support cations. This ligand effect governs the catalytic activity, which in turn modulates the reactivity of the surface molybdenum oxide overlayer. Ultimately, the reducibility of the bridging Mo—O—support bond determines the reaction rate during methanol oxidation[45].

Under that premise, it is feasible to assume that in the 2.5 MoO_3 catalyst, being under the theoretical monolayer, a new redox site (Mo – O – Ti) emerges, exhibiting similar characteristics to the classic redox site (Mo – O – Mo) previously reported[14]. In both cases, the rate – determining step occurs; however, this interfacial site could be responsible for retaining formaldehyde long enough to enable its dehydrogenation into formate, thereby altering the oxidative dehydrogenation pathway of methanol toward the production methyl formate.

To validate this hypothesis, Figure I–11 presents kinetic experiments in which the partial pressure of methanol varied at 225°C over the 2.5 and MoO_3, while keeping both the total flow and the O_2 partial pressure constant. Experiments were carried out under conditions where methanol conversion remained below 5%, thereby minimizing the equilibrium associated with DMM formation.

Fig. I–11.a displays the DMM formation rate, which exhibits the same trend for both catalysts, showing a quadratic increase with methanol partial pressure. Figure I–11.b illustrates the MF formation rate, which reveals the most distinctive behavior. For the 15 MoO_3 catalyst, MF formation increases nearly linearly with methanol partial pressure (approximately 0.9). In contrast, for the 2.5 MoO_3 catalyst, the MF formation rate does not follow either a linear or quadratic dependence on methanol pressure, instead suggesting a fractional reaction apparent order (0.44) with respect to methanol.

Under the premise that the rate–determining step for both products is the initial dehydrogenation of the methoxy group[14,39], that the 2.5 MoO_3 catalyst stabilizes surface

intermediates more strongly than 15 MoO_3 catalyst, and that distinct types of redox sites are involved, the most plausible explanation for the observed behavior is that DMM are mainly formed on Mo – O – Mo redox sites, whereas MF is produced on both Mo – O – Mo and Mo – O – Ti redox sites.

On the one hand, DMM exhibits a similar dependence on methanol pressure for both catalysts, and thus the same apparent reaction order, which suggests that its formation is governed by the same kinetic regime. This behavior implies that the kinetic expressions are dominated by a numerator proportional to methanol pressure squared, with no significant influence of site saturation or competitive adsorption terms. Nevertheless, this apparent second – order dependence can also be rationalized by considering the scenario proposed by Galdames et al.[39]. In their work, they proposed a kinetic model involving a hemiacetal intermediate and two types of active sites (redox and acid sites). The rate – determining step for the formation of the three products (FA, MF and DMM) was identified as the first dehydrogenation of methanol, which defined the numerator of each kinetic expression. The denominator contains two terms that determine products selectivity, in addition to the site balance. The first term models the selectivity between DMM and MF, arising from the equilibrium between DMM and its intermediate that subsequently leads to MF. The second term corresponds to the selectivity between the desorption of FA and the formation of hemiacetal. Therefore, a denominator term could also contribute to increasing the apparent reaction order for both products. This term would originate from the competition experienced by surface formaldehyde species between desorption as a product or further transformation into intermediates leading to DMM or MF. As illustrated in Scheme 1, FA acts as a key precursor for the formation of DMM and MF in any of the proposed mechanistic pathways.

On the other hand, MF displays a markedly different behavior between the two catalysts. The fractional apparent order observed for 2.5 MoO_3 suggests that, in this case, the site – balance requires explicit consideration of surface intermediates. Under such conditions, the microkinetic expressions derived from the elementary steps naturally introduce methanol pressure–dependent terms in the denominator. In contrast, for the 15 MoO_3 catalyst, the assumption of a lower coverage of intermediates leads to a denominator close to unity, resulting in a nearly linear dependence on methanol pressure.

This difference supports the site–balance hypothesis discussed earlier and reinforces the notion that two distinct types of redox sites participate in the partial oxidation of methanol over MoO_3/TiO_2 catalysts.

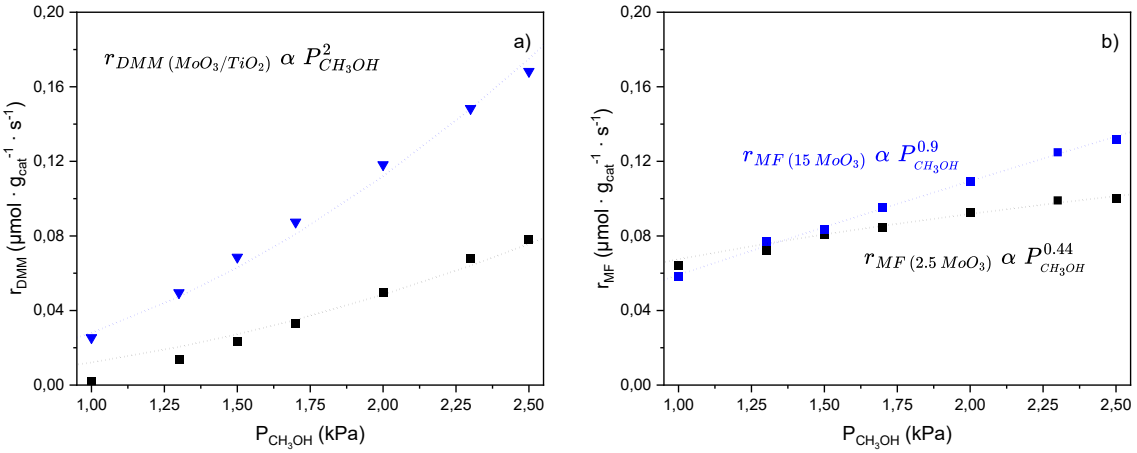

Figure I–11 Effect of methanol partial pressure on products formation rates at 225°C over 2.5 MoO_3 (black) and 15 MoO_3 (blue) catalysts. Reaction conditions: P_{O2} = 9 kPa, P_{Ar} = 10 kPa, N_2 balance, total flow = 60 ml/min, catalyst mass: 2.5 MoO_3 = 50 mg and 15 MoO_3 = 20 mg. a) Dimethoxymethane formation rate and b) Methyl formate formation rate.

Building on the kinetics trends observed for DMM and MF, and considering the insights gained from the transient and isotopic labeling experiments, the distinct roles of Mo – O – Mo and Mo – O – Ti sites in governing the reaction pathways can be elucidated. While Mo – O – Mo redox sites lead to DMM and MF formation following the hemiacetal pathway, the interfacial Mo – O – Ti redox sites steer methanol oxidation toward MF through the formate – based mechanism. This interpretation not only rationalizes the distinct kinetics dependencies observed between the 2.5 and 15 MoO_3 catalysts but also provides a coherent framework to understand the influence of surface intermediates and kinetic isotope effects on products distribution.

By questioning mechanistic hypotheses from the literature through Operando spectroscopic and isotopic transient experiments under controlled conditions, and by correlating structural features with product distribution, this study clarifies the role of titania in methyl formate formation and integrates the proposed mechanism into a coherent reaction scheme. Catalysts that contain oligomeric Mo oxide and exposed TiO_2 stabilize surface intermediates and, via interfacial Mo – O – Ti redox sites, promote methyl formate formation through the formate pathway. In contrast, catalysts that present predominantly crystalline domains, Mo – O – Mo, produce methyl formate predominantly via the hemiacetal route. Over these latter catalysts, IR monitoring indicates that surface intermediates do not accumulate significantly, reflecting the intrinsic instability of the hemiacetal intermediate, which prevents its accumulation and causes the reaction to restart essentially from zero upon methanol reintroduction.

Transient and isotopic labeling experiments quantitatively rule out methoxy exchange and, in parallel, the Tishchenko route under our conditions. The consistent formation of

$HCOOCD_3$ during $CD_3OD \rightarrow CH_3OH$ transition supports the kinetic relevance of both hemiacetal and formate intermediates. A kinetic isotope effect explains the observed predominance of $HCOOCD_3$ and, together with differences in intermediate stabilization and site balance, accounts for the distinct apparent reaction orders and selectivity trends.

Altogether, these results provide a unified mechanistic picture linking MoO_3 structure, the nature of redox sites, intermediate stabilization, and isotopic kinetics, establishing a solid reference framework for comparison with other redox systems (particularly V_2O_5/TiO_2) examined in the following chapter.

Chapter II: Characterization and mechanistic investigation of active sites in methanol oxidation over vanadium catalysts using transient *Operando* - DRIFTS

Upon obtaining transient results with MoO_3/TiO_2 catalysts, a natural question arose: are these findings reproducible in other catalysts, such as vanadium–based ones, which have been extensively studied in the oxidative dehydrogenation of methanol and from the basis of most mechanistic studies?

These vanadium oxide catalysts also marked the starting point of this line of research in CarboCat, prior to the transition toward molybdenum–based catalysts. To address this question, additional materials were designed and characterized using techniques capable of identifying the different types of bonds present in the active sites, allowing for the evaluation of reproducibility and a deeper understanding of the reaction mechanisms.

The section concludes with the presentation of the answer to the question posed, alongside the corresponding analysis and its implications, illustrating how the results contribute to a more comprehensive view of the processes under study.

II. 1. Experimental

II.1.1. Catalysts preparation

Three V_2O_5/TiO_2 catalysts with different vanadium loadings (2.5, 15 and 25 atom V nm^{-2} theorical) were synthesized by wet impregnation following the procedure reported by Santander et al[46]. Ammonium metavanadate (NH_4VO_3) and oxalic acid (in a 1:2 molar ratio) were used as vanadium precursors to enhance metal dispersion over the TiO_2 support. The resulting solids were dried and calcined at 500 °C for 4 h.

II.1.2. Catalysts Characterization

The crystalline structure of the catalysts was examined by X-ray diffraction (XRD) using an X-ray diffractometer Bruker D4 Endeavor (Billerica, USA) equipped with a solid-state detector (LynxEye) using Cu Kα radiation (λ = 0.154 nm).

Textural properties were determined from N_2 adsorption–desorption isotherms at 77 K using a Gemini VII Surface Area Analyzer Micromeritics (Georgia, USA). Prior to the experiments, the samples were degassed at 300 °C under N_2 flow (Airliquide 99.999 %). Surface area was calculated from the BET equation.

The redox behavior of the catalysts was investigated by temperature – programmed reduction with hydrogen (H_2-TPR), providing insight into the reducibility of vanadium species and their interaction with the TiO_2 support. Measurements were carried out in a ChemBet 3000

Pulsar TPR/TPD (Quantachrome), heating under a diluted H_2/Ar (9.94% vol. H_2, Linde) flow up to 800 °C at 5 °C min^{-1}, while monitoring H_2 consumption with a thermal conductivity detector (TCD).

The surface exposure of TiO_2 was further quantified through methanol adsorption experiments following the methodology of Broomhead et al[24]. These tests were conducted in a fixed-bed reactor at 150 °C under a 0.1% methanol stream (60 ml min^{-1}), conditions that suppress methanol oxidation and ensure surface-limited adsorption. Given that methanol adsorption occurs predominantly on TiO_2 Lewis acid sites, the vanadia contribution was considered negligible. The amount of adsorbed methanol, referenced to pure TiO_2, was used to estimate the fraction of exposed TiO_2 in each catalyst.

II.1.3. Catalytic activity measurements

Kinetic measurements of the V_2O_5/TiO_2 catalysts were performed following the same procedure described in Chapter 1 for MoO_3/TiO_2. Briefly, the catalysts were tested in a fixed-bed reactor under identical conditions, with the catalyst diluted in quartz sand to prevent heat and mass transfer limitations. Pretreatment, reactant flows, and CH_3OH/O_2 ratios were identical to those previously described. Unlike the Mo-based experiments, the concentration of reactants and reaction products was monitored exclusively by a Extorr XT-100 residual gas analyzer (RGA), instead of the SRI 8610C gas chromatograph used previously.

II.1.4. Operando – DRIFTS

Operando diffuse reflectance infrared Fourier transform spectroscopy (DRIFTS) experiments were conducted as in Chapter 1, using the same reactor cell, spectrometer configuration, gas flows, and experimental sequences—including isotopic experiments with CH_3OH and CD_3OD—applied to the V_2O_5/TiO_2 catalysts.

By applying identical experimental protocols, with only the detection method updated, the catalytic behavior of V_2O_5/TiO_2 can be directly compared to that of MoO_3/TiO_2, allowing for a consistent evaluation of the influence of the metal oxide identity on methanol oxidation and surface intermediates.

II. 2. Results and Discussion

II.2.1 Characterization

Figure II–1 shows the XRD patterns of the 2.5, 15 and 25 V_2O_5/TiO_2 catalysts, with the corresponding crystallographic planes of vanadium pentoxide indicated for the 25 V_2O_5 sample[39]. No crystalline vanadium phases were detectable for 2.5 and 15 V_2O_5, whereas 25 V_2O_5 displays well-defined peaks corresponding to crystalline V_2O_5, with the most intense reflection assigned to the (110) plane.

The absence of detectable vanadium crystallinity in 15 V_2O_5 catalyst does not exclude the presence of nanocrystalline domains. Previous reports indicate that vanadium surface density around 15 V/nm^2 typically corresponds to partially crystalline structures[15,24,39,46], and the lack of XRD peaks likely arises from crystallite sizes below the detection limit of the technique (~5 nm).

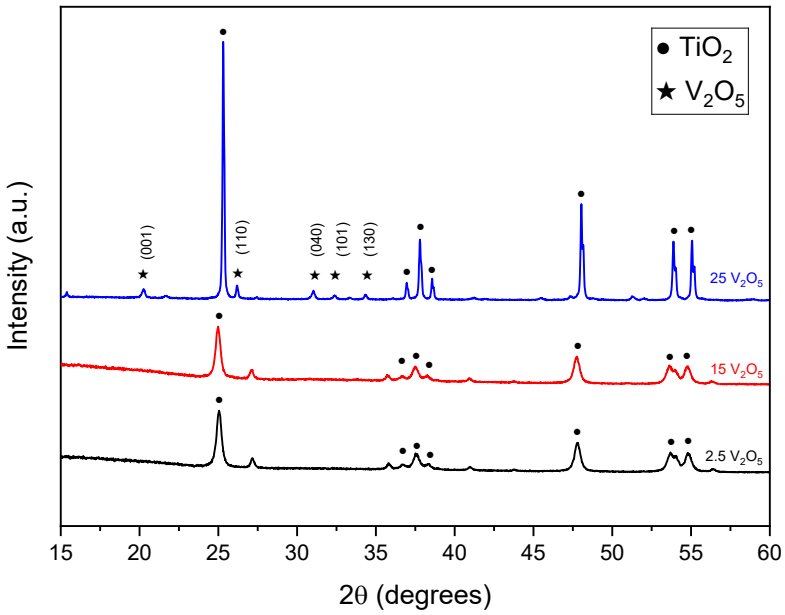

Figure II–1 XRD patterns of V_2O_5/TiO_2 as a function of vanadium surface density. Circles (●) correspond to anatase phase of TiO_2, while stars (★) correspond to diffraction peaks attributed to vanadium phases on V_2O_5 crystals.

N_2 physisorption measurements (BET) revealed a marked decrease in specific surface area with increasing vanadium loading. The 2.5 V_2O_5 catalyst exhibits 53 m²/g, comparable to that of bare TiO_2, whereas 15 V_2O_5 decreased to 43 m²/g, and 25 V_2O_5 shows a drastic drop to 8 m²/g. These results suggest that higher vanadium loadings promote particle aggregation and/or extensive surface coverage of TiO_2, thereby reducing the accessible surface area and potentially influencing catalytic performance.

Figure II–2 presents the H_2-TPR profiles of the three V_2O_5/TiO_2 catalysts. A clear shift of the reduction peaks toward higher temperatures is observed with increasing vanadium loading: 2.5 V_2O_5 exhibits a maximum at 440 °C, 15 V_2O_5 at 450 °C, while 25 V_2O_5 displays two distinct reductions peaks at 520 °C and 610 °C. In contrast, the onset of reduction follows the opposite trend, occurring at approximately 330 °C for 2.5 V_2O_5, 260 °C for 25 V_2O_5 and as low as 215 °C for 15 V_2O_5.

These features indicate that crystalline vanadium species are more difficult to reduce than dispersed monomeric ones, in line with previous reports by Besselmann et al[47]. The appearance of two reduction peaks for 25 V_2O_5, reflects the presence of multiple reducible vanadium environments associated with higher vanadium loadings, as also described by Briand et al[48].

The lower reduction onset temperature observed for 15 V_2O_5 suggests a higher proportion of labile surface oxygen species and enhanced redox activity at mild temperatures[49]. In contrast, although 2.5 V_2O_5 reduces at higher temperatures, it undergoes more extensive reduction at intermediate temperature than 25 V_2O_5, indicating a greater overall reducibility of dispersed VO_x species compared to bulk – like crystalline V_2O_5.

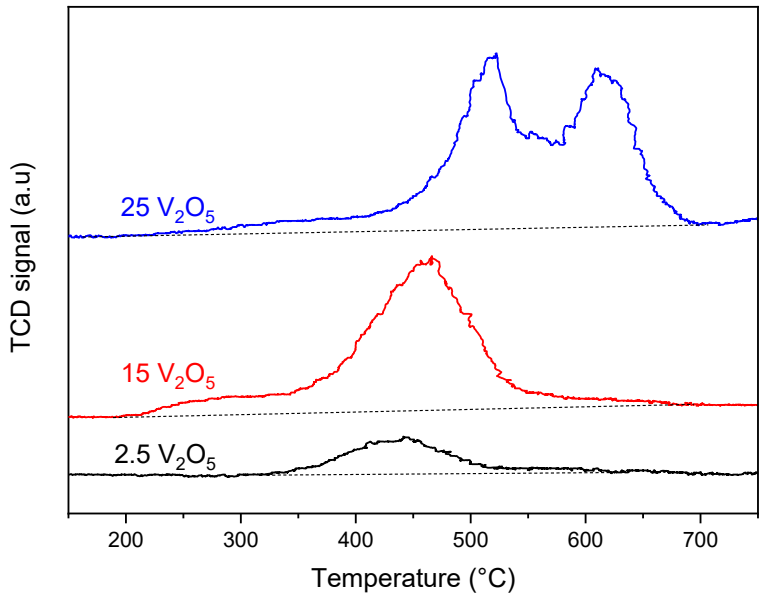

Figure II–2 H_2-temperature programmed reduction for all supported V_2O_5/TiO_2 catalysts.

By integrating the area under the reduction profiles, the molar ratio of H_2 consumed to vanadium was determined for each catalyst. In a complete reduction process, vanadium in V_2O_5 is expected to undergo a two – electron transition from V^{5+} to V^{3+}, corresponding to a

theoretical H_2/V ratio of 2:1[50]. The 25 V_2O_5 sample approaches this theoretical value expected for complete reduction, 2.0; while 2.5 and 15 V_2O_5 exhibit higher H_2/V ratios of 4.0 and 2.4, respectively. These deviations indicate additional reduction pathways beyond the stoichiometric vanadium reduction.

Such behavior is consistent with Mars–Van Krevelen mechanisms[24,51], in which partial reduction of the TiO_2 support regenerates vanadium through V–O–Ti linkages. Accordingly, the 2.5 V_2O_5 catalyst likely contains a high fraction of dispersed surface V–O–Ti species, allowing each vanadium atom to undergo two reductions. The first reduction step involves the removal of interfacial oxygen, either those directly bonded to vanadium or belonging to the vanadia layer itself. The second reduction arises from lattice oxygens of titania, which migrate to refill the oxygen vacancy generated on the metal center[24].

The intermediate ratio of 15 V_2O_5 suggests a mixed contribution of V–O–Ti and V–O–V environments, whereas the near – stoichiometric ratio of 25 V_2O_5 reflects a predominance of crystalline V–O–V domains. These observations are fully consistent with the XRD results, which indicate increasing crystallinity with vanadium loading.

Figure II–3 presents the methanol adsorption profiles obtained for TiO_2 and the V_2O_5/TiO_2 catalysts with increasing vanadium loading. In these experiments, methanol was first passed through a bypass line until a steady–state signal was achieved; at t = 0, the flow was redirect through the catalyst bed via a three – way valve, initiating the adsorption process. A pronounced drop in the methanol signal is observed immediately after the switch, corresponding to surface adsorption. The magnitude of this drop (highlighted by the segmented baseline) decreases markedly with increasing vanadium content: TiO_2 exhibits the largest adsorption capacity, followed by 2.5, 15 and finally 25 V_2O_5, which shows only minimal adsorption.

Integration of the adsorption profiles, following the methodology proposed by Broomhead et al.,[24] allowed quantification of methanol uptake and estimation of the exposed TiO_2 surface area. Relative to bare TiO_2, methanol adsorption decreases by approximately 20%, 70%, and 95% for 2.5, 15, and 25 V_2O_5, respectively. These results confirm that methanol adsorption occurs predominantly on TiO_2 and that higher vanadium domains progressively block these sites, in agreement with XRD and BET analyses.

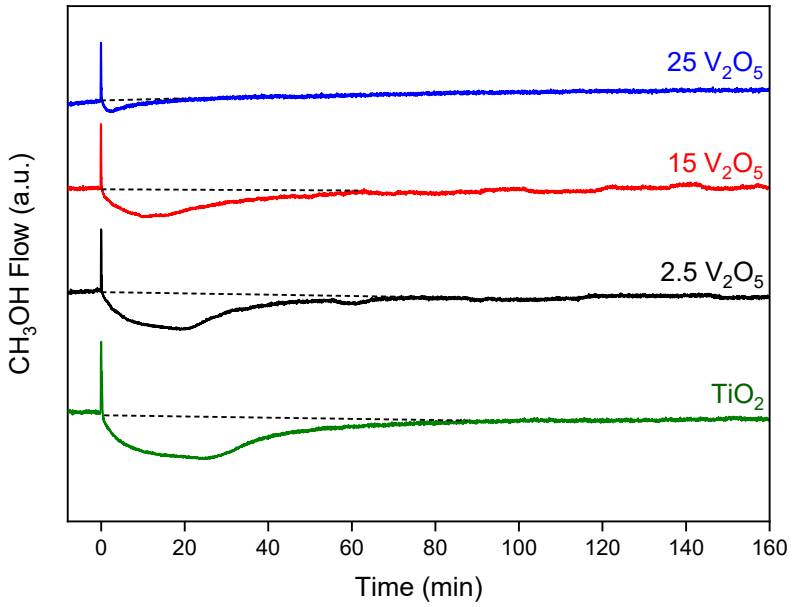

Figure II–3 Methanol adsorption profiles of TiO_2 and V_2O_5/TiO_2 catalysts.

Because the extent of methanol adsorption is directly related to the fraction of exposed TiO_2 surface, it is relevant to consider how VO_x domain structure evolves with loading. Scheme II–1 and Table II–1 provide a schematic overview of the different VO_x structures supported on titania, highlighting the types of lattice oxygen associated with each configuration per exposed V^{5+} site, based on the work of Broomhead et al[24]. As shown in this Scheme, VO_x domains contain three types of lattice oxygen (O^I – O^{III}) defined by their coordination: O^I as V–O–Ti interfacial bridges, O^{II} as V–O–V bridges, and O^{III} as terminal V=O groups. Their relative abundance varies with domain size: isolated monovanadates are richer in O^I, polyvanadates incorporate all three oxygen types with increasing O^{II} as domains grow, and multilayer structures resemble crystalline V_2O_5 surfaces dominated by O^{II} and lacking surface accessible O^I. This structural evolution, from monomeric to polymeric and multilayer VO_x species, has been consistently identified through Raman spectroscopy, X–ray adsorption and HR – TEM[24].

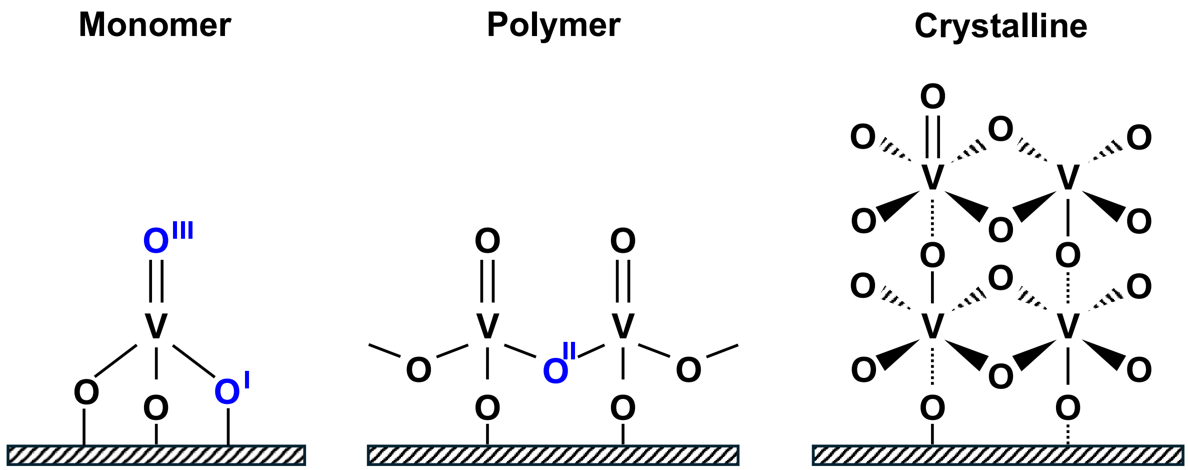

Scheme II–1 Schematic illustration of the dispersed VO_x monomer, polymer and crystalline moieties on TiO_2 and their active oxygen atoms O^I (V–O–Ti), O^{II} (V–O–V) and O^{III} (V=O) per exposed V^{5+} cation[24].

Table II–1 Coordinated oxygen per exposed V^{5+}.

	Monomer	Polymer	Crystalline
O^I	3	1	0
O^{II}	0	2 – 4	5
O^{III}	1	1	0.5

The quantitative analysis of methanol adsorption provides an estimate of the exposed TiO_2 surface, which in turn enables calculation of the surface density of VO_x species (Table II–2). When interpreted in the context of the structural motifs summarized in Scheme II–1, the calculated VO_x densities reveal clear structural differences among the catalysts. These differences in domain size also imply distinct distributions of O^I, O^{II}, and O^{III} lattice oxygen, consistent with the trends expected for isolated, polymeric, and multilayer VO_x structures and in line with the TPR–H_2 results. The full derivation of the quantitative calculations, specifically, those used to obtain VO_x structures densities and the corresponding active oxygen atoms densities, is provided in Appendix A. II–3.

The 2.5 V_2O_5 catalyst exhibits predominantly monomeric vanadium species (≈3.2 VO_x/nm^2) consistent with an extensive presence of V–O–Ti linkages and high surface exposed of titania. In contrast, 15 V_2O_5 catalyst exhibits mainly crystalline domains (≈0.6 VO_x/nm^2 polymeric and 0 VO_x/nm^2 monomeric), indicating partial aggregation of vanadium species into sub–nanometric crystallites. Finally, 25 V_2O_5 catalyst is fully crystalline, with high crystal density and negligible V–O–Ti contributions, consistent with its low methanol uptake and near-stoichiometric H_2 consumption in TPR.

Analysis of lattice oxygen densities (O^I, O^{II}, O^{III}) further supports this structural evolution. Monomeric VO_x species are enriched in interfacial O^I oxygens, whereas polymeric VO_x species exhibit a mixed O^I – O^{III} distribution, and crystalline VO_x contains mostly O^{II} oxygen. Table II–2 shows a pronounced decrease in O^I with increasing vanadium loading and a sharp rise in O^{II} between 15 and 25 V_2O_5, reflecting crystal growth and the onset of XRD detectable phases.

Table II–2 Quantitative results of methanol adsorption, exposed TiO_2 surface, and calculated surface densities of VO_x species and lattice oxygens for V_2O_5/TiO_2 catalysts.

Catalysts	Adsorbed CH_3OH (μmol/g)	Exposed superficial titania (%)	Monomer density (VO_x/nm^2)	Polymer density (VO_x/nm^2)	Crystal density (VO_x/nm^2)	ρ_{s-O^I} (O^I / nm^2)	$\rho_{s-O^{II}}$ (O^{II}/ nm^2)	$\rho_{s-O^{III}}$ (O^{III}/ nm^2)
TiO_2	2500	100	-	-	-	-	-	-
2.5 V_2O_5	2000	80	3.22	0.62	0	10.3	2.4	3.8
15 V_2O_5	790	31	0	0.6	11.1	0.6	58	6
25 V_2O_5	130	5	0	0	116	0	577	58

Collectively, methanol adsorption, TPR-H_2, and oxygen density analyses provide consistent evidence of the progressive structure evolution of vanadium oxide species: 2.5 V_2O_5 is primarily monomeric with localized polymeric domains; 15 V_2O_5 exhibits a partially crystalline structure (< 5 nm crystallites); and 25 V_2O_5 is fully crystalline.

II.2.2 Catalytic activity

Figure II–4 displays the catalytic activity of 2.5, 15 and 25 V_2O_5/TiO_2 catalysts as function of temperature, obtained from fixed–bed reactor experiments.

Fig. II–4.a shows methanol conversion, where 2.5 and 15 V_2O_5 exhibit an increase in activity with vanadium loading, consistent with literature reports[15,24,39]. However, the 25 V_2O_5 catalyst shows a significant decrease in conversion, which can be associated with its lower surface area and the predominance of bulk V_2O_5 domains. The higher activity of the 15 V_2O_5 catalyst agrees well with its higher reducibility observed in TPR–H_2 experiments (Figure II–2), while the poorer performance of 25 V_2O_5 demonstrate its limited redox capacity.

Fig II–4.b–d presents the yields of FA, DMM and MF as a function of temperature, respectively. The 15 V_2O_5 catalyst exhibits the highest yields of MF and DMM, confirming its superior redox and acid balance. Notably, DMM formation peaks appear at a lower temperature than for the other samples, indicating higher activity at mild conditions. In

contrast, this catalyst produces the lowest yield of FA among the three samples. The 2.5 V_2O_5 catalyst displays intermediate yields, following a similar trend to 15 V_2O_5, but with lower overall performance, suggesting that it does not yet reach the optimal vanadium loading. On the other hand, the 25 V_2O_5 catalyst presents the opposite behavior: it shows the lowest DMM and MF yields and the highest FA yield. The decrease in DMM yield at mild temperatures is attributed to the equilibrium of its formation, while the decline in MF and FA yields results from the onset of complete oxidation pathways, leading to the formation of CO and CO_2.

Based on these results, the lower DMM and MF yields observed for 25 V_2O_5 can be attributed to the close proximity of V_2O_5 clusters, a direct consequence of its reduced surface area. This structural arrangement promotes the rapid desorption of FA from the surface, preventing its subsequent transformation into DMM and MF. As discussed in chapter 1, formaldehyde acts as a key intermediate in the formation of both products, and its premature desorption interrupts the reaction sequence. Therefore, these findings reinforce the notion that FA competes between desorption and further surface reaction, rather than participating through a gas–phase mechanism. This evidence (now obtained on vanadium-based catalysts) further supports that the conversion of FA into DMM and MF occurs predominantly through adsorbed surface intermediates, highlighting the need to include a kinetic term that accounts for this mechanistic competition, which may increase or decrease the apparent order reaction of the products.

On the other hand, the 2.5 and 15 V_2O_5 catalyst presents similar trends in the yields of methanol partial oxidation products, suggesting that their differences are primarily structural rather than mechanistic. Nevertheless, comparisons with the MoO_3/TiO_2 catalysts discussed in Chapter 1 reveal an important distinction, the transition from oligomeric to crystalline structures led to marked differences in product distribution associated with mechanistic changes. For V_2O_5/TiO_2 catalysts, however, the product trends remain consistent between these loadings, implying that while both materials share similar surface intermediates, the mechanism of methanol oxidation over vanadia likely proceeds through a single dominant pathway modulated by structural effects rather than a fundamental mechanistic shift. This observation suggests that the vanadium redox centers remain catalytically active throughout the loading range, but their spatial distribution and local environment determine the relative selectivity toward FA, MF and DMM.

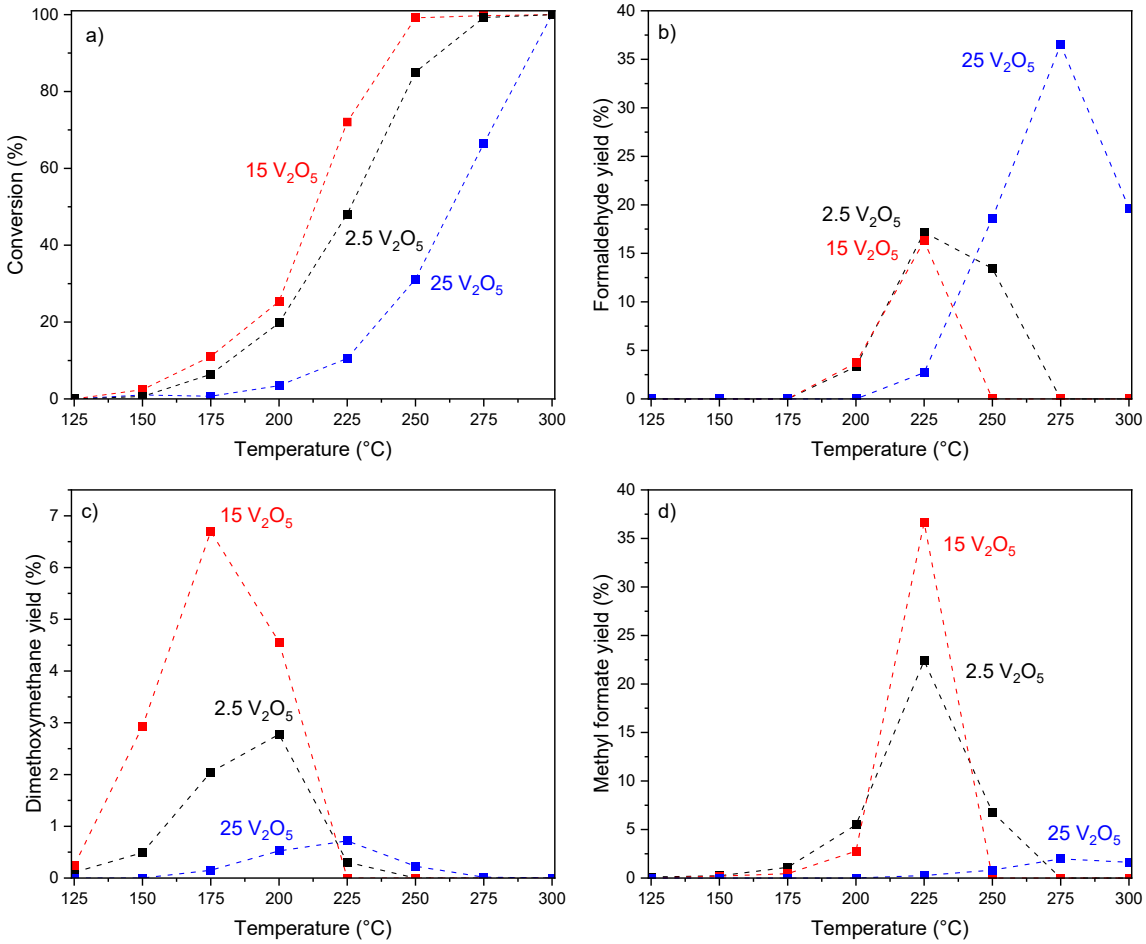

Figure II–4 a) Conversion and yield of b) FA, c) DMM and d) MF for the V_2O_5/TiO_2 samples (black for 2.5 V_2O_5, red for 15 V_2O_5 and blue for 25 V_2O_5) as a function of temperature (GHSV = 19 L h^{-1} g_{cat}^{-1}, $CH_3OH/O_2/Ar/N_2$ (feed) = 4/9/10/77 %v/v).

Although these steady–state results suggest a structurally modulated yet mechanistically uniform behavior, they also raise fundamental questions about the nature of the active sites, and the participation of the different surface oxygen species present in the catalyst. The apparent continuity in product distribution with increasing vanadium loading could conceal subtle differences in the dynamics of intermediate formation and transformation. To unravel these aspects, transient and isotopic experiments become essential tools to directly probe the reactivity of surface species and the involvement of lattice oxygen in the redox cycle. The following section addresses these questions, aiming to determine whether the methanol oxidation mechanism over vanadia truly follows a single pathway or if distinct kinetic regimes emerge under dynamic conditions.

II.2.3 Operando – DRIFTS measurements

Figure II – 5 and II – 6 show the transient experiments at 225°C when alternating the feed between CH_3OH and CD_3OD, over the 2.5 and 15 V_2O_5/TiO_2 catalysts, emphasizing the evolution of methyl formate and its isotopologues. Upon switching from hydrogenated to deuterated methanol (H → D transition, Fig. II – 5a and 6a), a rapid decrease in the signal corresponding to fully hydrogenated methyl formate ($HCOOCH_3$, H-MF) is observed immediately after the helium drop. Shortly thereafter, the predominant isotopologue formed is methyl formate containing a deuterated methoxy group ($HCOOCD_3$). Toward the end of the transition, the signal of fully deuterated methyl formate ($DCOOCD_3$, D-MF) appears.

This behavior resembles that observed during the same transition over the MoO_3/TiO_2 catalysts, shown in Figure I–3a and I–4a of Chapter 1. As previously discussed, the formation of the $HCOOCD_3$ is consistent with the reaction pathway involving HCOO* or CH_3OCH_2OH intermediates. Conversely, the isotopologue associated with the Tishchenko reaction, $HCOOCHD_2$, was not detected in these catalysts either. Therefore, the Tishchenko pathway can be ruled out as a significant pathway for MF formation in both metal oxide systems, which display analogous isotopic behavior.

On the other hand, Figure II – 5b and II – 6b show the CD_3OD → CH_3OH transition. Upon replacing CD_3OD with CH_3OH in the feed, the helium signal rises sharply and simultaneously, the signal corresponding to $DCOOCD_3$ decreases, while a few seconds later, the fully hydrogenated MF begins to increase. Between these two extremes, partially hydrogenated species emerge, and it is in this region where the main differences between the catalysts become evident.

For the 2.5 V_2O_5 catalyst, $DCOOCH_3$ remains the dominant species throughout the transition, indicating a product distribution consistent with the formate or hemiacetal mechanism. Also, the distribution and the behavior of the MF isotopologues is similar that observed during both transition (Figure II – 5a and 5b). In contrast, the 15 V_2O_5 catalyst exhibits a clear predominance of $HCOOCD_3$, deviating the expected isotopic progression. Although $DCOOCH_3$ is also formed, its intensity remains noticeably lower than that of $HCOOCD_3$. This inversion indicates the participation of an isotopic effect, as previously described and discussed in Chapter 1.

The evidence supporting the presence of an isotopic effect in the 15 V_2O_5 catalyst lies in the markedly higher intensity of the $HCOOCD_3$ signal during the D → H transition compared to that observed in the reverse H → D transition. As discussed in Chapter 1, the more favorable dehydrogenation of the C–H bond relative to C–D allows hydrogenated methanol to react with deuterated methoxy groups that remained adsorbed on the surface, resulting in a pronounced formation of $HCOOCD_3$. Interestingly, the intensity of the $HCOOCD_3$ signal detected during the H → D transition is similar to that of $DCOOCH_3$ in the D → H transition,

further demonstrating, from a complementary standpoint, the isotopic effect operating on this catalyst.

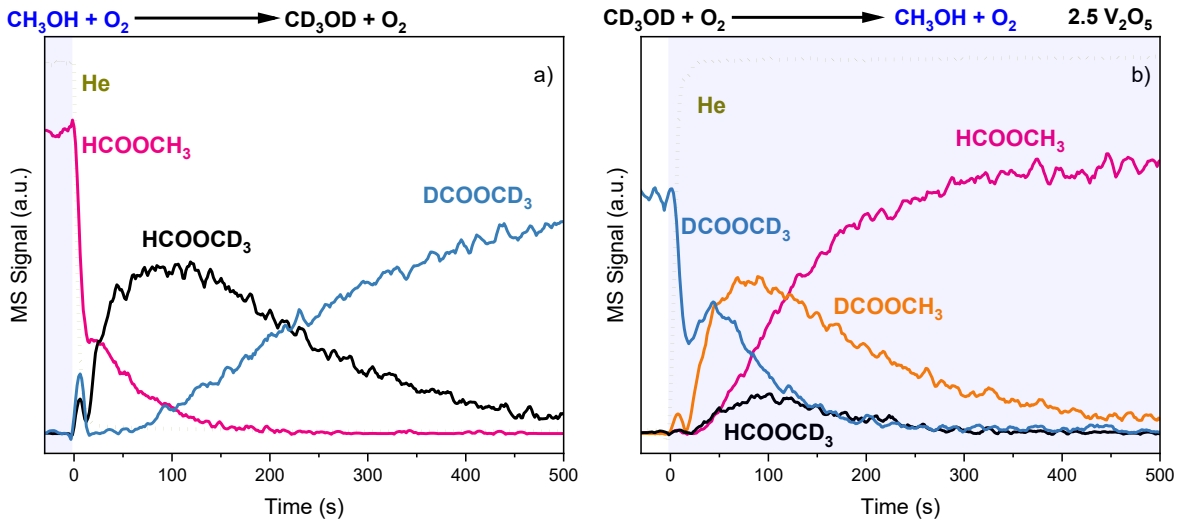

Figure II–5 MS signal of methyl formate (hydrogenated, partially, and fully deuterated) in the $CH_3OH/O_2/N_2/Ar/He \rightarrow CD_3OD/O_2/N_2/Ar \rightarrow CH_3OH/O_2/N_2/Ar/He$ transition at 225°C for 2.5 V_2O_5 catalyst during a) $CH_3OH \rightarrow CD_3OD$ transition; and b) $CD_3OD \rightarrow CH_3OH$ transition.

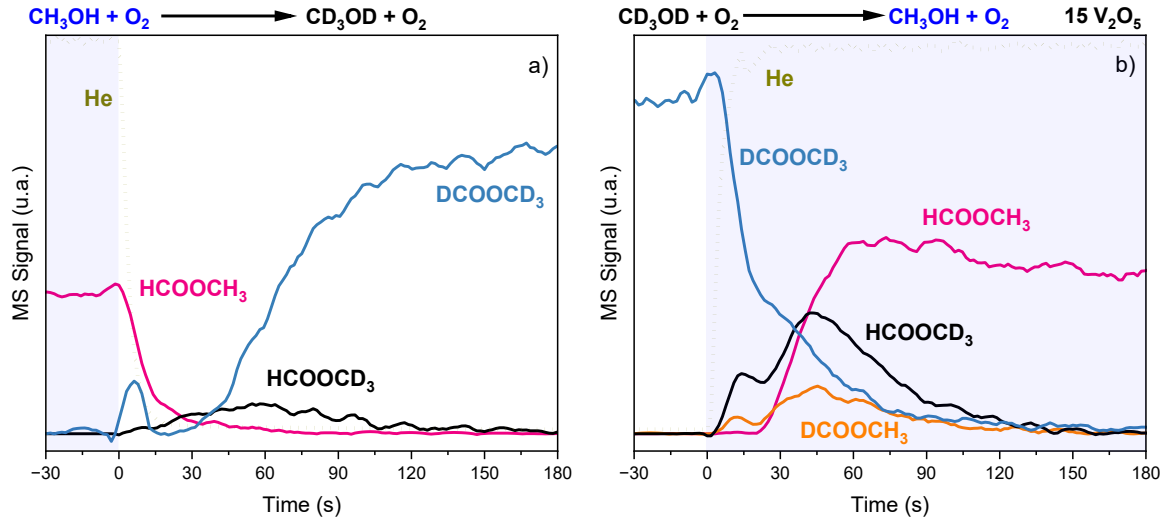

Figure II–6 MS signal of methyl formate (hydrogenated, partially, and fully deuterated) in the $CH_3OH/O_2/N_2/Ar/He \rightarrow CD_3OD/O_2/N_2/Ar \rightarrow CH_3OH/O_2/N_2/Ar/He$ transition at 225°C for 15 V_2O_5 catalyst during a) $CH_3OH \rightarrow CD_3OD$ transition; and b) $CD_3OD \rightarrow CH_3OH$ transition.

Figure II–7 and II–8 display the evolution of the IR spectra during $CH_3OH/O_2/N_2/Ar/He \rightarrow CD_3OD/O_2/N_2/Ar$ (a) and $CD_3OD/O_2/N_2/Ar \rightarrow CH_3OH/O_2/N_2/Ar/He$ (b) transitions for the 2.5 V_2O_5 and 15 V_2O_5 catalysts respectively, focusing one the first two minutes after the feed switch. The spectra in green represent the steady – state before the change, while those in blue correspond to spectra recorded 2 minutes after switching. Three characteristic regions can be distinguished: H-methoxy (2800 – 3000 cm^{-1}), D-methoxy (2000 – 2300 cm^{-1}) and formates species (1300 – 1600 cm^{-1}). In both transitions, the evolution of H- and D-methoxy bands is remarkably clean.

In contrast to the MoO_3/TiO_2 catalysts discussed in Chapter 1, where no surface formate species were detected as steady state conditions, the V_2O_5/TiO_2 materials clearly exhibit bands attributable to surface formates under steady – state conditions. For the 2.5 V_2O_5 catalyst (Fig. II–7), these species show remarkable dynamic behavior, undergoing complete isotopic exchange between hydrogenated and deuterated formates within approximately five minutes. In the case of the 15 V_2O_5 catalyst (Fig. II–8), weak bands in the formate region can also be distinguished; however, their low intensity and partial overlap with other species make their assignment less conclusive, resembling the behavior previously observed for the molybdenum – based catalysts.

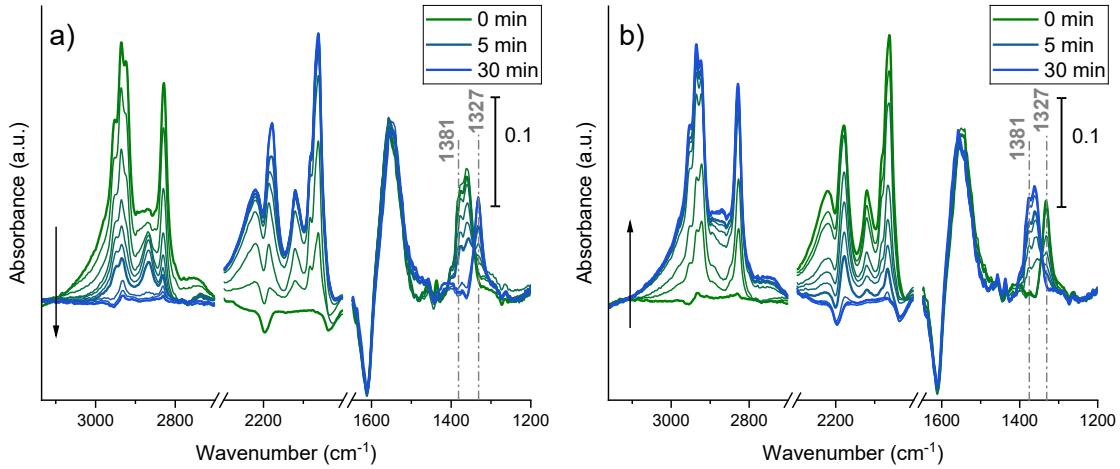

Figure II–7 IR spectra for 2.5 V_2O_5/TiO_2 catalyst at 225°C during a) $CH_3OH/O_2/N_2/Ar/He \rightarrow CD_3OD/O_2/N_2/Ar$ transition; b) $CD_3OD/O_2/N_2/Ar \rightarrow CH_3OH/O_2/N_2/Ar/He$ transition.

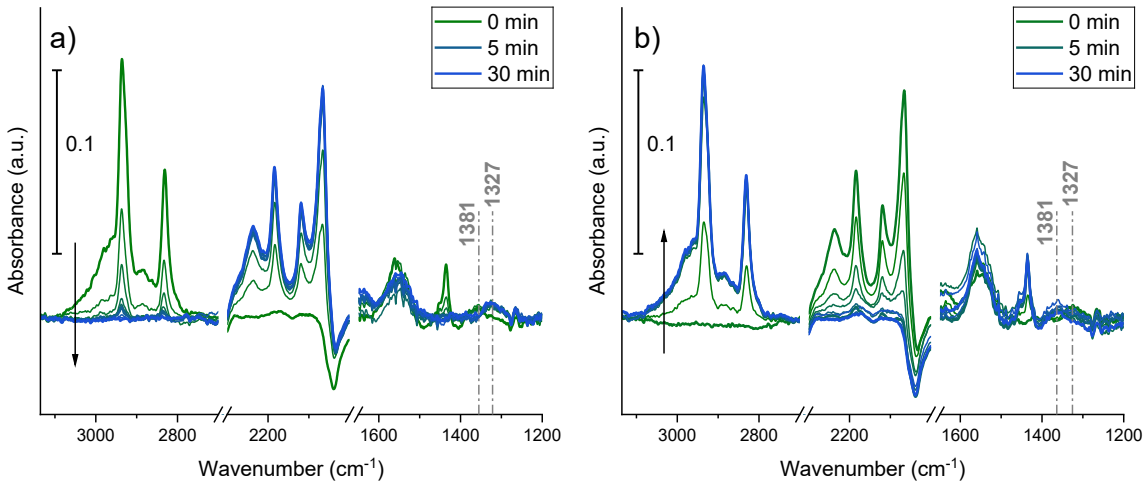

Figure II–8 IR spectra for 15 V_2O_5/TiO_2 catalyst at 225°C during a) $CH_3OH/O_2/N_2/Ar/He \rightarrow CD_3OD/O_2/N_2/Ar$ transition; b) $CD_3OD/O_2/N_2/Ar \rightarrow CH_3OH/O_2/N_2/Ar/He$ transition.

In line with the previous discussion, Figure II – 9 presents an *operando* analysis of the methyl formate and its isotopologues detected by MS, along with their correlation to the temporal evolution of the surface species identified by IR spectroscopy, both datasets normalized, during the $CH_3OH/O_2/N_2/Ar/He \rightarrow CD_3OD/O_2/N_2/Ar$ transition.

Figure II–9a shows the decreases in the $HCOOCH_3$ signal along with the decline of the hydrogenated methoxy (H-methoxy, 2925 cm^{-1}) and formate (H-formate, 1362 cm^{-1}) bands. From this Figure, it is evident that the $HCOOCH_3$ signal drops sharply at the beginning of the transition due to the valve switch, in contrast with the more gradual response of the surface methoxy species. However, at a later stage, the $HCOOCH_3$ profile exhibits a change in slope, becoming comparable to that of the hydrogenated methoxy groups. Notably, the decrease in hydrogenated formate species does not follow the same trend as that of hydrogenated MF.

Figure II–9b displays the transient formation of the partially deuterated methyl formate isotopologue ($HCOOCD_3$) and the evolution of the hydrogenated formate and deuterated methoxy species (D-methoxy, 2064 cm^{-1}). In this case, it can be observed that the rise in the formation of partially deuterated MF is slightly faster than the accumulation of CD_3O* species on the surface. At the same time, the decay of the hydrogenated formates occurs in parallel with the decrease of $HCOOCD_3$. Based on these observations, and in connection with the results in Fig. II–9a, it can be inferred that the MF formation mechanism on this catalyst follows an Eley–Rideal pathway, involving the coupling of methanol with the key intermediate – formate. The fact that the hydrogenated formates, unequivocally detected on the surface, decay concurrently with the partially deuterated isotopologue provides compelling evidence that MF is indeed formed through surface formates. Moreover, the earlier decrease of CH_3O* species compared to that of the HCOO* suggests that a fraction

of these methoxy groups undergo dehydrogenation to yield formates, passing through the RDS in the process.

Figure II–9c depicts the formation of fully deuterated methyl formate (D-MF) and the evolution of the deuterated methoxy and formate (D-formate, 1327 cm^{-1}). Similar to the behavior observed in Fig. II–9b, formates begin to accumulate on the surface in parallel with the detection of D-MF. The fact that $DCOOCD_3$ formation occurs simultaneously with the build–up of surface formates, and after the accumulation of CD_3O* species further confirms that the kinetically relevant step involves the interconversion between methoxy and formate intermediates, while the subsequent coupling with methanol proceeds rapidly once formates are formed.

Consistent results were obtained from the reverse isotopic switch ($CD_3OD/O_2/N_2/Ar$ → $CH_3OH/O_2/N_2/Ar/He$), whose full analysis is presented in Appendix A. II. 2 and reproduces the same correlations between gas–phase MF isotopologues and surface intermediates described in Fig. II–9.

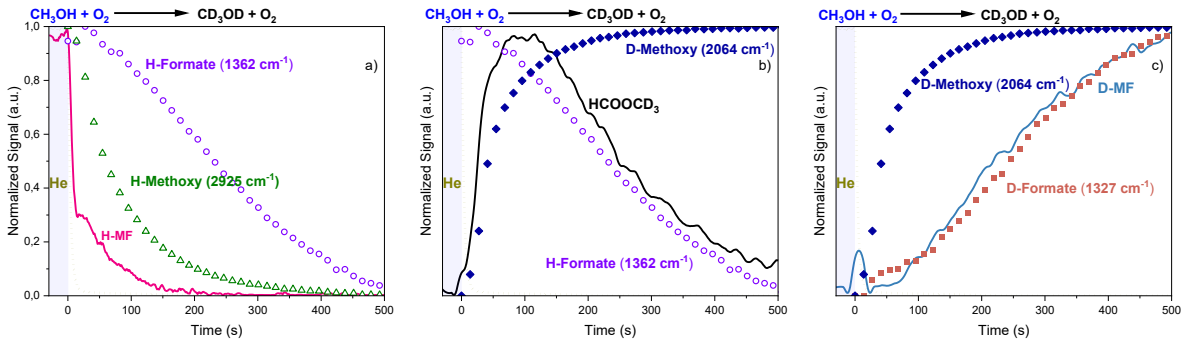

Figure II–9 *Operando* IR-MS analysis during the $CH_3OH/O_2/N_2/Ar/He$ → $CD_3OD/O_2/N_2/Ar$ transition over the 2.5 V_2O_5/TiO_2 catalyst at 225°C. (a) $HCOOCH_3$ and the evolution of the IR surface species associated with its formation: hydrogenated methoxy (2925 cm^{-1}) and formate (1362 cm^{-1}). (b) $HCOOCD_3$ and the evolution of the IR surface species associated with its formation: deuterated methoxy (2064 cm^{-1}) and hydrogenated formate (1362 cm^{-1}). (b) $DCOOCD_3$ and the evolution of the IR surface species associated with its formation: deuterated methoxy (2064 cm^{-1}) and formate (1327 cm^{-1}).

Together, the results presented in Figure II-9, along with the temporal correspondence between the MS and IR signal during both forward and reverse transitions, consistently confirm that the formation of methyl formate over the 2.5 V_2O_5 catalyst proceeds through surface formate species. Once generated, these HCOO* rapidly react with the CH_3OH to yield $HCOOCH_3$ and its isotopologues. This behavior suggests that the system reaches an operational equilibrium between formate formation and consumption, demonstrating that

under steady–state reaction conditions, these species are both stable and actively involved in MF formation.

Regarding the 15 V_2O_5/TiO_2 catalyst, as shown in Figure II-8, the detection of surface formates in the analyzed spectral regions exhibits a slight shift; however, the band intensity is not sufficiently strong to enable an *operando* analysis comparable to that performed for the 2.5 V_2O_5 catalysts. Nevertheless, considering that the 15 V_2O_5 catalyst showed the highest yield toward MF, two possibilities arise: first, that due to its higher activity, the formates generated under steady–state conditions possess a very short lifetime on the surface; or second, that the formation of MF in this sample proceeds predominantly through the hemiacetal pathway. To discern which of these hypotheses applies, the same experimental strategy developed in Chapter 1 will be employed. This approach, previously used to elucidate the operative mechanism on molybdenum–based catalysts, where no surface formates were detected under steady–state conditions, consists of transient experiments designed to promote and track the potential formation of surface species. After reaching steady–state reaction conditions, a purge step is carried out to remove methanol from the gas phase, leaving the adsorbed species on the surface. Subsequently, deuterated methanol is introduced (without oxygen in the feed), allowing the identification of the MF isotopologues formed and, consequently, the determination of which surface intermediates participate in their formation.

Figure II-10 shows the transient responses at 175°C for the 2.5 (II-10a) and 15 (II-10b) V_2O_5/TiO_2 catalysts during $CH_3OH + O_2 \rightarrow N_2 \rightarrow CD_3OD$ sequence (blue background for the first step, red for the second and white for last step). During this transition, the normalized gas–phase evolution of $HCOOCH_3$ and $HCOOCD_3$ was analyzed to evaluate the behavior of both catalysts. The $HCOOCH_3$ signal in the gas phase decreased upon replacing $CH_3OH + O_2$ with N_2 in both samples, and when the feed was switched to CD_3OD, the $HCOOCD_3$ signal appeared in the gas phase.

The main difference observed between the catalysts in this Figure lies in the maximum points of MF production throughout the transition. For the 2.5 V_2O_5 catalyst, the maximum MF yield, through the partially deuterated product $HCOOCD_3$, was reached upon introducing deuterated methanol. It is noteworthy that the intensity of this maximum of MF, represented by the $HCOOCD_3$ isotopologue during the CD_3OD step, is only slightly higher than the steady–state production of $HCOOCH_3$ shown in Fig. II–10a. Considering the results of the previous transient experiment, in which this catalyst was shown to produce MF predominantly via the formate pathway, this modest increase suggests that, in addition to its surface stability (as previously discussed), the formate intermediate attains a relatively high surface coverage under these conditions.

In contrast, the 15 V_2O_5 catalyst exhibited its maximum MF production under steady–state conditions, displaying only a negligible $HCOOCD_3$ peak during the introduction of CD_3OD. Given that the hemiacetal is an unstable surface intermediate, it cannot account for the formation of partially deuterated MF. Therefore, the minor peak observed can only be attributed to surface formates, which is plausible considering that this catalyst presents a small fraction of exposed surface titania, as inferred from the methanol adsorption results, and that the experiment was carried out under relatively low–temperature conditions, favoring the coverage and inhibiting the desorption of these intermediates. Nevertheless, since this catalyst shows the highest overall MF yield among all samples, the contribution of the formate route must be limited. Consequently, it can be reasonably concluded that MF formation on the 15 V_2O_5 catalyst proceeds predominantly through the hemiacetal mechanism.

Further evidence supporting these interpretations arises from the results obtained with molybdenum–based catalysts discussed in Chapter 1. When the same transient experiment was performed on those samples, identical trends were observed, leading to the same mechanistic conclusions. It is also worth noting that the molybdenum catalysts exhibited a greater structural depth and morphological complexity compared to the vanadium counterparts. Therefore, these consistent observations suggest a broader tendency among metal–oxide catalysts toward similar reactions behavior under comparable conditions.

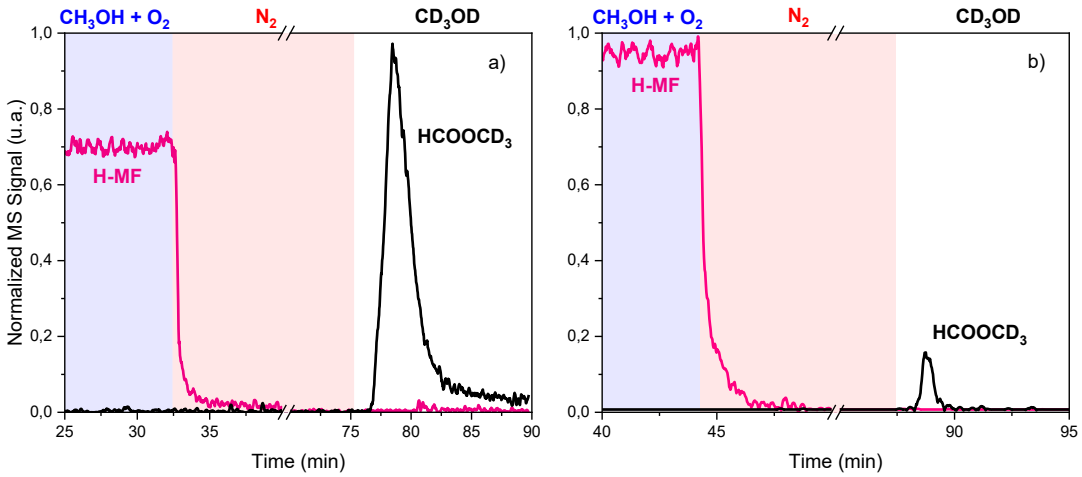

Figure II–10 Normalized MS signal for hydrogenated methyl formate ($HCOOCH_3$, H-MF) and its partially isotopologue ($HCOOCD_3$) during the transition $CH_3OH + O_2 \rightarrow N_2 \rightarrow CD_3OD$ at 175°C for the a) 2.5 V_2O_5 catalyst and b) 15 V_2O_5 catalyst. Fully deuterated MF is not shown for the sake of simplicity.

To complement the previous discussion, Figure II-11 and II-12 show the continuous IR monitoring of surface intermediates throughout the $N_2 \rightarrow CD_3OD$ transition for the 2.5 and 15 V_2O_5 catalysts, respectively. The bands analyzed correspond to hydrogenated methoxy

(2925 cm^{-1}), hydrogenated formates (1360 cm^{-1}), and deuterated methoxy (2064 cm^{-1}). Regarding the methoxy species (H- and D-), they exhibit the expected behavior throughout the different stages of the experiment. Upon removal of the CH_3OH feed, the surface CH_3O* species are consumed, whereas the introduction of deuterated methanol leads to the progressive accumulation of CD_3O* species on both catalysts surface.

For both catalysts, the consumption of CH_3O* species leads to the formation of HCOO*, with the evolution of this band revealing the main differences. For the 2.5 V_2O_5 catalyst, the formate species increase above their steady–state level and remain stable on the surface until the introduction of CD_3OD, at which point they are completely consumed. In contrast, for the 15 V_2O_5 catalyst, the formate bands initially increase but are desorbed or consumed from the catalyst surface after approximately 15 minutes, well before the introduction of deuterated methanol. Once CD_3OD is introduced, the remaining formates are fully consumed.

The behavior of surface species on the 2.5 V_2O_5 catalyst is consistent with and reinforces the observations from Figure II-10, as evidenced by the increase in formate bands followed by their consumption upon the introduction of deuterated methanol. In contrast, the 15 V_2O_5 catalyst exhibits a transient, volcano–like behavior in the formate bands, occurring out of sync with the deuterated methanol feed. The formation of formate intermediates on 15 V_2O_5 is plausible, given the presence of a small fraction of exposed titania, which could provide interfacial sites for their generation. However, considering the minimal steady–state intensity of the formate bands and the negligible $HCOOCD_3$ production during this transition, there is no supporting evidence for a formate–mediated MF formation pathway on this catalyst. These observations therefore reaffirm that, under steady–state conditions, MF formation on 15 V_2O_5 proceeds predominantly via the hemiacetal mechanism.

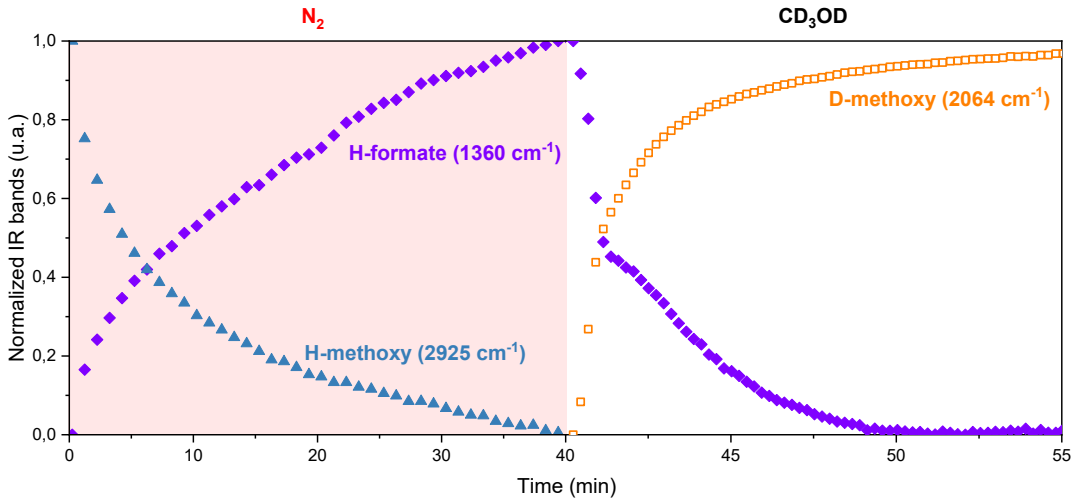

Figure II–11 Normalized IR signal of the evolution of the different intermediates on the surface H-methoxy bands: 2925 cm^{-1}; H-formate bands: 1360 cm^{-1}; D-methoxy bands: 2064

cm^{-1}; for the 2.5 V_2O_5 catalyst at 175 °C during N_2 (red background) → CD_3OD (white background) transition.

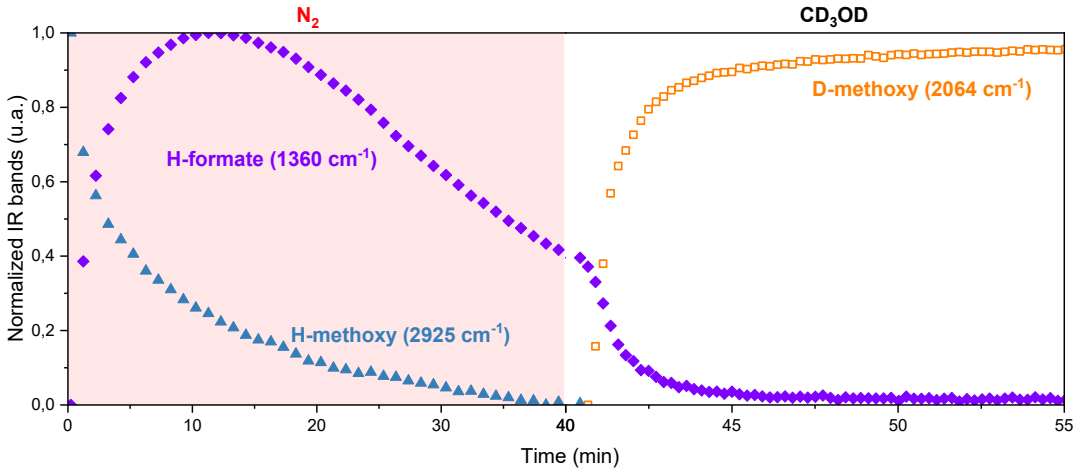

Figure II–12 Normalized IR signal of the evolution of the different intermediates on the surface H-methoxy bands: 2925 cm^{-1}; H-formate bands: 1360 cm^{-1}; D-methoxy bands: 2064 cm^{-1}; for the 15 V_2O_5 catalyst at 175 °C during N_2 (red background) → CD_3OD (white background) transition.

II.2.4. Overall discussion

To gain a comprehensive understanding of how surface structure governs reactivity in the methanol to methyl formate transformation, this section integrates insights from structural characterization, steady–state reactor experiments and transient, isotopic and spectroscopy analyses of the V_2O_5/TiO_2 catalysts.

For the 2.5 V_2O_5/TiO_2 catalyst, characterization results reveal a material with a high dispersion of vanadium oxide species over the titania surface. Approximately 80% of the exposed surface corresponds to TiO_2, and based on theoretical calculations, this composition should favor the presence of monomeric vanadium oxide species forming direct V–O–Ti linkages with the support. This structural configuration was further corroborated by temperature programmed reduction analysis, where the H_2 consumption reached a molar ratio of 4 mol H_2 per mol V, approximately twice the stoichiometric requirement expected for V^{5+} → V^{3+} reduction. This deviation indicates the participation of the support lattice: oxygen atoms from titania are mobilized to replenish vacancies formed on vanadium sites. Such behavior provides direct evidence of the presence of interfacial redox sites involving both metal and support atoms.

Taken together, these results demonstrate that the 2.5 V_2O_5/TiO_2 catalyst likely adopts a structural configuration analogous to that of the 2.5 MoO_3/TiO_2 sample, which was

previously studied in greater depth. In that case, the formation of interfacial M–O–Ti redox sites (M = Mo or V) was identified as a key feature governing the catalytic behavior, suggesting that similar sites are responsible for the distinctive activity observed in this vanadium–based material.

For the 15 V_2O_5/TiO_2 catalyst, the characterization results reveal a material with a significantly lower dispersion of vanadium oxide over the titania surface. According to theoretical estimations, this composition should favor the presence of crystalline vanadia domains, in contrast to the monomeric species predominant at lower loadings. Although not well–defined crystalline reflections were detected by XRD, this absence can be attributed to the formation of small vanadia crystallites, which might still preserve a minor fraction of interfacial vanadium sites. This hypothesis is supported by the TPR-H_2 results, which show a hydrogen consumption ratio of 2.4 mol H_2 per mol V, a value close to the stoichiometric reduction. The slight excess beyond the theoretical value suggests the contribution of a limited number of V–O–Ti linkages, consistent with the presence of a small amount of interfacial redox character.

Altogether, these findings indicate that the 15 V_2O_5/TiO_2 catalyst likely adopts a structural configuration analogous to that of the 15 MoO_3/TiO_2 sample, previously discussed in greater detail. In that case, the catalytic performance was associated with the predominance of crystalline M–O–M redox sites (M = Mo or V), where the reaction proceeds mainly through lattice–based redox cycles rather than through interfacial metal–support participation.

When analyzing the catalytic performance under identical operating conditions in the fixed–bed reactor, both 2.5 and 15 V_2O_5/TiO_2 catalysts exhibited essentially the same kinetic trends, characterized by a high yield toward methyl formate. Interestingly, the 2.5 V_2O_5 catalyst behaves as a non–optimized version of the 15 V_2O_5 sample: it reaches lower overall activity and MF yield yet follows an almost identical kinetic profile.

This observation contrasts sharply with the behavior previously reported for MoO_3/TiO_2 catalysts, where the structurally crystalline 15 MoO_3 sample displayed high selectivity toward formaldehyde, while the low loading 2.5 MoO_3 catalyst (dominated by interfacial redox sites) primarily favored MF formation. A comparable trend emerges within the vanadium series, as the full crystalline 25 V_2O_5/TiO_2 catalyst shifts the selectivity toward formaldehyde, reinforcing the link between crystalline and the preferred oxidation pathway.

The comparable kinetic performance observed for both vanadium–based catalysts could imply that structural redox sites have minimal influence on the operative mechanism. Yet, such an assumption neglects possible differences in the nature and dynamics of the surface intermediates. *Operando* isotopic transient experiments were therefore conducted to directly

monitor the evolution of surface intermediates during the MF production, proving insights into whether both catalysts follow a truly common mechanistic pathway.

These experiments unequivocally demonstrated the mechanistic divergence between both catalysts. For 2.5 V_2O_5, a clear dynamic evolution of surface formate species was observed. These intermediates, already present under steady–state conditions, evolved in perfect correlation with MF formation, establishing the formate route as the dominant pathway. In sharp contrast, the 15 V_2O_5 catalyst exhibited neither a stable population of formate species nor any evidence of their involvement in MF production. Therefore, the reaction on this catalyst must proceed predominantly through the hemiacetal mechanism.

This behavior aligns closely with that observed in molybdenum catalysts, suggesting that the type of redox site in metal oxide catalysts (transition metals), can be directly associated with the predominant mechanism responsible for MF formation.

Scheme II-2 illustrates the Mars – Van Krevelen cycle involved in the formation of methyl formate over interfacial and crystalline redox sites. Both catalytic cycles initiate with the adsorption of methanol onto the active site (step one), either as a molecularly adsorbed species on the crystalline site or as a methoxy intermediate on the interfacial site. In the subsequent rate-determining step (step two), hydrogen abstraction from the methoxy group occurs on both sites, followed by the formation and desorption of water, which generated an oxygen vacancy on the catalysts surface (step three). Up to this point, both mechanisms proceed through analogous elementary steps; the mechanistic divergence between the two types of active sites arises here.

As observed and discussed for the 2.5 V_2O_5/TiO_2 catalyst (interfacial redox site), oxygen migration from the support occurs to replenish the oxygen vacancy within the M–O–Ti linkage. In contrast, such migration is absent in the crystalline redox sites. For practical purposes, the oxygen vacancy in the crystalline sites can be considered to remain vacant; however, it could also be replenished by oxygen from the gas phase, since this step is quasi equilibrated.

Subsequently, in step four, the key intermediate for methyl formate production is formed. On the interfacial redox sites, once the oxygen vacancy has been replenished, the adsorbed formaldehyde undergoes an additional dehydrogenation step to yield formate species, the key intermediate in this cycle. Conversely, on the crystalline sites, during step four, methanol re–enters the cycle and reacts with formaldehyde to form a hemiacetal complex, which constitutes the dominant intermediate in this pathway. In step five, an inversion relative to the previous step occurs: methanol now enters the interfacial cycle and reacts with the surface formate species to produce MF, while on the crystalline site, the hemiacetal undergoes oxidative dehydrogenation to yield methyl formate.

In the subsequent steps, both cycles converge once again. In step six, methyl formate and water desorb from the surface, generating a new oxygen vacancy on the catalyst. Finally, in step seven, oxygen from the feed replenishes the vacancy, closing the catalytic cycles and restoring the active sites for continuous operation.

This mechanistic scheme highlights the fundamental role of the redox site nature in dictating the dominant reaction pathway. Such a structure – reactivity correlation underscores the universality of this behavior across transition metal oxide systems.

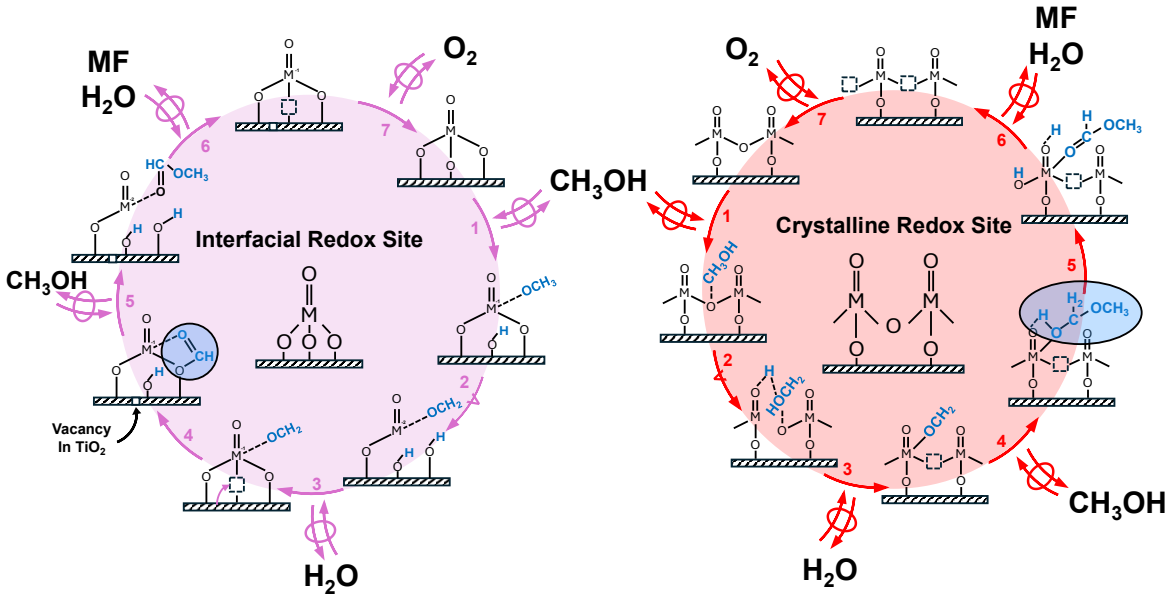

Scheme II-2 Proposed Mars – Van Krevelen mechanism for methyl formate formation over titania supported MoO_3 and V_2O_5 catalysts, distinguishing interfacial (pink) and crystalline (red) redox sites.

Conclusions

The combined mechanistic, structural, and kinetic evidence presented throughout this work provides a unified picture of methanol oxidative dehydrogenation over MoO_3/TiO_2 and V_2O_5/TiO_2 catalysts, highlighting the decisive role of surface structure in dictating reactivity and selectivity.

For both metal oxides, two distinct types of redox sites were identified: interfacial M–O–Ti linkages and crystalline M–O–M domains (M = Mo, V). These sites define two parallel Mars–Van Krevelen cycles that govern the formation of methyl formate and dimethoxymethane.

Catalysts dominated by interfacial redox sites, characterized by high dispersion and a significant contribution of titania to the surface composition, stabilize formates species and promote methyl formate formation through the formate pathway. In these systems, reversible oxygen transfer between the metal oxide and titania sustains the catalytic cycle, enabling the participation of interfacial oxygen atoms in the redox turnover.

Conversely, catalysts dominated by crystalline redox sites, where extended metal–oxygen–metal connectivity prevails, favor the hemiacetal route, in which less–stabilized surface intermediates lead directly to the formation of methyl formate and dimethoxymethane. The limited accumulation of surface intermediates observed under *operando* conditions reflects the intrinsic reactivity of this pathway.

Transient and isotopic labeling experiments conclusively ruled out the Tishchenko route as a viable for methyl formate formation under our conditions. This exclusion is not biased by potential methoxy exchange processes, which were independently demonstrated to be absent. Moreover, the lack of formaldehyde readsorption on the Lewis acid sites of titania, once it desorbs from the redox centers further supports this conclusion, confirming that surface formate species emerge as the dominant intermediates leading to methyl formate formation.

Altogether, these findings confirm the initial hypothesis that the formation of methyl formate and dimethoxymethane on transition–metal oxide catalysts supported on titania depends critically on the nature of the redox site involved. The interfacial M–O–Ti linkages act as structural and electronic bridges that enable oxygen mobility and intermediate stabilization, whereas crystalline M–O–M networks promote a more direct oxidative pathway with limited surface coverage.

This structural – mechanistic correlation provides a coherent framework that not only rationalizes the behavior of MoO_3/TiO_2 and V_2O_5/TiO_2 catalysts but also establishes a

general paradigm applicable to other reducible metal oxide systems involved in selective oxidation reactions.

Future Perspectives

The results of this thesis lay the groundwork for the development of a comprehensive kinetic model describing the formaldehyde, methyl formate and dimethoxymethane over transition metal oxide. By integrating kinetic data from both molybdenum- and vanadium-based systems and explicitly accounting for M–O–M and M–O–Ti redox sites, such a model would enable the generalization of structure, activity and selectivity relationships across a broad class of selective oxidation catalysts.

In parallel, future research should continue the rational modulation of the support to refine redox site structure and oxygen mobility. While titania remains the most effective support for methyl formate formation, the incorporation of redox active oxides such as SnO_2, CeO_2 or ZrO_2 into titania – based materials represent a promising strategy to enhance M–O–support interactions while maintaining efficient metal dispersion and suppressing total oxidation pathways.

Finally, within the context of the energy transition, further evaluation of dimethoxymethane and methyl formate as hydrogen carriers is warranted, given their increasing relevance in sustainable organic energy platforms.

References

(1) Garcia, G.; Arriola, E.; Chen, W.-H.; De Luna, M. D. A Comprehensive Review of Hydrogen Production from Methanol Thermochemical Conversion for Sustainability. *Energy* **2021**, *217*, 119384. https://doi.org/10.1016/j.energy.2020.119384.

(2) Hasan, M. M. F.; Rossi, L. M.; Debecker, D. P.; Leonard, K. C.; Li, Z.; Makhubela, B. C. E.; Zhao, C.; Kleij, A. Can CO_2 and Renewable Carbon Be Primary Resources for Sustainable Fuels and Chemicals? *ACS Sustain Chem Eng* **2021**, *9* (37), 12427–12430. https://doi.org/10.1021/acssuschemeng.1c06008.

(3) Olajire, A. A. Valorization of Greenhouse Carbon Dioxide Emissions into Value-Added Products by Catalytic Processes. *Journal of CO_2 Utilization* **2013**, *3–4*, 74–92. https://doi.org/10.1016/j.jcou.2013.10.004.

(4) Olah, G. A. Beyond Oil and Gas: The Methanol Economy. *Angewandte Chemie International Edition* **2005**, *44* (18), 2636–2639. https://doi.org/10.1002/anie.200462121.

(5) Sheetal; Mehara, P.; Das, P. Methanol as a Greener C_1 Synthon under Non-Noble Transition Metal-Catalyzed Conditions. *Coord Chem Rev* **2023**, *475*, 214851. https://doi.org/10.1016/j.ccr.2022.214851.

(6) Edwards, J.; Nicolaidis, J.; Cutlip, M. B.; Bennet, C. O. Methanol Partial Oxidation at Low Temperature. *J Catal* **1977**, *50* (1), 24–34. https://doi.org/10.1016/0021-9517(77)90005-7.

(7) Reuss, G.; Disteldorf, W.; Gamer, A. O.; Hilt, A. Formaldehyde. In *Ullmann's Encyclopedia of Industrial Chemistry*; Wiley-VCH Verlag GmbH & Co. KGaA: Weinheim, Germany, 2000. https://doi.org/10.1002/14356007.a11_619.

(8) Rong, L.; Xu, Z.; Sun, J.; Guo, G. New Methyl Formate Synthesis Method: Coal to Methyl Formate. *Journal of Energy Chemistry* **2018**, *27* (1), 238–242. https://doi.org/10.1016/j.jechem.2017.07.015.

(9) Ai, M. The Production of Methyl Formate by the Vapor-Phase Oxidation of Methanol. *J Catal* **1982**, *77* (1), 279–288. https://doi.org/10.1016/0021-9517(82)90168-3.

(10) Hu, H.; Wachs, I. E. Catalytic Properties of Supported Molybdenum Oxide Catalysts: In Situ Raman and Methanol Oxidation Studies. *J Phys Chem* **1995**, *99* (27), 10911–10922. https://doi.org/10.1021/j100027a035.

(11) Deo, G.; Wachs, I. E. Reactivity of Supported Vanadium Oxide Catalysts: The Partial Oxidation of Methanol. *J Catal* **1994**, *146* (2), 323–334. https://doi.org/10.1006/jcat.1994.1071.

(12) Liu, H.; Iglesia, E. Selective Oxidation of Methanol and Ethanol on Supported Ruthenium Oxide Clusters at Low Temperatures. *Journal of Physical Chemistry B* **2005**, *109* (6), 2155–2163. https://doi.org/10.1021/jp0401980.

(13) Kwon, S.; Deshlahra, P.; Iglesia, E. Dioxygen Activation Routes in Mars-van Krevelen Redox Cycles Catalyzed by Metal Oxides. *J Catal* **2018**, *364*, 228–247. https://doi.org/10.1016/j.jcat.2018.05.016.

(14) Deshlahra, P.; Carr, R. T.; Chai, S. H.; Iglesia, E. Mechanistic Details and Reactivity Descriptors in Oxidation and Acid Catalysis of Methanol. *ACS Catal* **2015**, *5* (2), 666–682. https://doi.org/10.1021/cs501599y.

(15) Kaichev, V. V.; Popova, G. Y.; Chesalov, Y. A.; Saraev, A. A.; Zemlyanov, D. Y.; Beloshapkin, S. A.; Knop-Gericke, A.; Schlögl, R.; Andrushkevich, T. V.; Bukhtiyarov, V. I. Selective Oxidation of Methanol to Form Dimethoxymethane and Methyl Formate over a Monolayer V_2O_5/TiO_2 Catalyst. *J Catal* **2014**, *311*, 59–70. https://doi.org/10.1016/j.jcat.2013.10.026.

(16) Busca, Guido.; Elmi, A. S.; Forzatti, Pio. Mechanism of Selective Methanol Oxidation over Vanadium Oxide-Titanium Oxide Catalysts: A FT-IR and Flow Reactor Study. *J Phys Chem* **1987**, *91* (20), 5263–5269. https://doi.org/10.1021/j100304a026.

(17) Busca, G. Infrared Studies of the Reactive Adsorption of Organic Molecules over Metal Oxides and of the Mechanisms of Their Heterogeneously-Catalyzed Oxidation. *Catal Today* **1996**, *27* (3–4), 457–496. https://doi.org/10.1016/0920-5861(95)00162-X.

(18) Elmi, A. S.; Tronconi, E.; Cristiani, C.; Gomez Martin, J. P.; Forzatti, P.; Busca, G. Mechanism and Active Sites for Methanol Oxidation to Methyl Formate over Coprecipitated Vanadium-Titanium Oxide Catalysts. *Ind Eng Chem Res* **1989**, *28* (4), 387–393. https://doi.org/10.1021/ie00088a002.

(19) Cairati, L.; Trifirò, F. SiO_2 and Al_2O_3 as Oxidation Catalysts of Methanol. *J Catal* **1983**, *80* (1), 25–30. https://doi.org/10.1016/0021-9517(83)90225-7.

(20) Wachs, I. E.; Madix, R. J. The Oxidation of Methanol on a Silver (110) Catalyst. *Surf Sci* **1978**, *76* (2), 531–558. https://doi.org/10.1016/0039-6028(78)90113-9.

(21) Tatibouët, J.-M.; Lauron-Pernot, H. Transient Isotopic Study of Methanol Oxidation on Unsupported V_2O_5. *J Mol Catal A Chem* **2001**, *171* (1–2), 205–216. https://doi.org/10.1016/S1381-1169(01)00104-2.

(22) LOUIS, C. Catalytic Properties of Silica-Supported Molybdenum Catalysts in Methanol Oxidation: The Influence of Molybdenum Dispersion. *J Catal* **1988**, *109* (2), 354–366. https://doi.org/10.1016/0021-9517(88)90218-7.

(23) Sambeth, J.; Juan, A.; Gambaro, L.; Thomas, H. Catalytic Oxidation of CH_3OH to $HCOOCH_3$ on V_2O_5: A Theoretical Study. *J Mol Catal A Chem* **1997**, *118* (3), 283–291. https://doi.org/10.1016/S1381-1169(96)00900-4.

(24) Broomhead, W. T.; Tian, W.; Herrera, J. E.; Chin, Y. H. C. Kinetic Coupling of Redox and Acid Chemistry in Methanol Partial Oxidation on Vanadium Oxide Catalysts. *ACS Catal* **2022**, *12* (19), 11801–11820. https://doi.org/10.1021/acscatal.2c01852.

(25) Cai, G.; Broomhead, W. T.; Chin, Y. H. C.; Cai, H. Advanced Kinetic and Titration Strategies for Assessing the Intrinsic Kinetics on Oxide and Sulfide Catalysts. *Top Catal* **2023**, *66* (15–16), 1102–1119. https://doi.org/10.1007/s11244-023-01849-w.

(26) Li, N.; Wang, S.; Sun, Y.; Li, S. First Principles Studies on the Selectivity of Dimethoxymethane and Methyl Formate in Methanol Oxidation over V_2O_5/TiO_2-Based Catalysts. *Physical Chemistry Chemical Physics* **2017**, *19* (29), 19393–19406. https://doi.org/10.1039/c7cp02326j.

(27) Liu, H.; Iglesia, E. Selective One-Step Synthesis of Dimethoxymethane via Methanol or Dimethyl Ether Oxidation on $H_{3+n}V_nMo_{12-n}PO_{40}$ Keggin Structures. *Journal of Physical Chemistry B* **2003**, *107* (39), 10840–10847. https://doi.org/10.1021/jp0301554.
(28) Ai, M. The Reaction of Formaldehyde on Various Metal Oxide Catalysts. *J Catal* **1983**, *83* (1), 141–150. https://doi.org/10.1016/0021-9517(83)90037-4.
(29) Galdames, G.; Fuentes, B.; Gómez, D.; Concepción, P.; Jiménez, R.; Karelovic, A. Unveiling the Pathways and Site Requirements of Methanol Oxidative Dehydrogenation on MoO_3/TiO_2 Catalysts: An Operando-FTIR Study. *J Catal* **2025**, *447*, 116094. https://doi.org/10.1016/j.jcat.2025.116094.
(30) Wachs, I. E. Raman and IR Studies of Surface Metal Oxide Species on Oxide Supports: Supported Metal Oxide Catalysts. *Catal Today* **1996**, *27* (3–4). https://doi.org/10.1016/0920-5861(95)00203-0.
(31) Groff, R. An Infrared Study of Methanol and Ammonia Adsorption on Molybdenum Trioxide. *J Catal* **1984**, *86* (1), 215–218. https://doi.org/10.1016/0021-9517(84)90363-4.
(32) Ouyang, F.; Kondo, J. N.; Maruya, K.; Domen, K. IR Study on H/D Isotope Exchange Reactions of Formate and Methoxy Species with D_2 on ZrO_2. *Journal of the Chemical Society, Faraday Transactions* **1997**, *93* (1), 169–174. https://doi.org/10.1039/a604962a.
(33) Burcham, L. J.; Badlani, M.; Wachs, I. E. The Origin of the Ligand Effect in Metal Oxide Catalysts: Novel Fixed-Bed in Situ Infrared and Kinetic Studies during Methanol Oxidation. *J Catal* **2001**, *203* (1), 104–121. https://doi.org/10.1006/jcat.2001.3312.
(34) Burcham, L. J.; Badlani, M.; Wachs, I. E. The Origin of the Ligand Effect in Metal Oxide Catalysts: Novel Fixed-Bed in Situ Infrared and Kinetic Studies during Methanol Oxidation. *J Catal* **2001**, *203* (1), 104–121. https://doi.org/10.1006/jcat.2001.3312.
(35) Suda, Y.; Morimoto, T. Molecularly Adsorbed Water on the Bare Surface of Titania (Rutile). *Langmuir* **1987**, *3* (5), 786–788. https://doi.org/10.1021/la00077a037.
(36) N.W. Cant; S.P. Tonner; D.L. Trimm; M.S. Wainwright. Isotopic Labeling Studies of the Mechanism of Dehydrogenation of Methanol to Methyl Formate over Copper-Based Catalysts. *J Catal* **1985**, *91* (2), 197–207. https://doi.org/10.1016/0021-9517(85)90334-3.
(37) Takahashi, K.; Takezawa, N.; Kobayashi, H. Mechanism of Formation of Methyl Formate from Formaldehyde over Copper Catalysts. *Chem Lett* **1983**, *12* (7), 1061–1064. https://doi.org/10.1246/cl.1983.1061.
(38) Pearson, D. M.; Waymouth, R. M. Mechanistic Studies of the Oxidative Dehydrogenation of Methanol Using a Cationic Palladium Complex. *Organometallics* **2009**, *28* (13), 3896–3900. https://doi.org/10.1021/om900217s.
(39) Galdames, G.; Santander, P.; Jiménez, R.; Karelovic, A. A Detailed Kinetic Model for the Methanol Oxidative Dehydrogenation on Vanadia-Based Catalysts: Aggregation State Role and Active Site Requirements. *Appl Catal A Gen* **2024**, *682*, 119807. https://doi.org/10.1016/j.apcata.2024.119807.

(40) Tatibouët, J. M. Methanol Oxidation as a Catalytic Surface Probe. *Appl Catal A Gen* **1997**, *148* (2), 213–252. https://doi.org/10.1016/S0926-860X(96)00236-0.
(41) Badlani, M.; Wachs, I. E. Methanol: A "Smart" Chemical Probe Molecule. *Catal Letters* **2001**, *75* (3–4), 137–149. https://doi.org/10.1023/A:1016715520904.
(42) Kecskés, T.; Raskó, J.; Kiss, J. FTIR and Mass Spectrometric Studies on the Interaction of Formaldehyde with TiO2 Supported Pt and Au Catalysts. *Appl Catal A Gen* **2004**, *273* (1–2), 55–62. https://doi.org/10.1016/j.apcata.2004.06.012.
(43) Chen, X.; He, G.; Li, Y.; Chen, M.; Qin, X.; Zhang, C.; He, H. Identification of a Facile Pathway for Dioxymethylene Conversion to Formate Catalyzed by Surface Hydroxyl on TiO_2 -Based Catalyst. *ACS Catal* **2020**, *10* (17), 9706–9715. https://doi.org/10.1021/acscatal.0c01901.
(44) Tian, H.; Ross, E. I.; Wachs, I. E. Quantitative Determination of the Speciation of Surface Vanadium Oxides and Their Catalytic Activity. *J Phys Chem B* **2006**, *110* (19), 9593–9600. https://doi.org/10.1021/jp055767y.
(45) Burcham, L. J.; Badlani, M.; Wachs, I. E. The Origin of the Ligand Effect in Metal Oxide Catalysts: Novel Fixed-Bed in Situ Infrared and Kinetic Studies during Methanol Oxidation. *J Catal* **2001**, *203* (1), 104–121. https://doi.org/10.1006/jcat.2001.3312.
(46) Santander, P.; Bravo, L.; Pecchi, G.; Karelovic, A. The Consequences of Support Identity on the Oxidative Conversion of Furfural to Maleic Anhydride on Vanadia Catalysts. *Appl Catal A Gen* **2020**, *595*. https://doi.org/10.1016/j.apcata.2020.117513.
(47) Besselmann, S.; Freitag, C.; Hinrichsen, O.; Muhler, M. Temperature-Programmed Reduction and Oxidation Experiments with V_2O_5/TiO_2 Catalysts. *Physical Chemistry Chemical Physics* **2001**, *3* (21), 4633–4638. https://doi.org/10.1039/b105466j.
(48) Briand, L. E.; Gambaro, L.; Thomas, H. Temperature-Programmed Reduction of V_2O_5 and Coprecipitated $V_2O_5{-}TiO_2$ by Hydrogen. *Journal of Thermal Analysis* **1995**, *44* (4), 803–821. https://doi.org/10.1007/BF02547266.
(49) Wachs, I. E.; Weckhuysen, B. M. Structure and Reactivity of Surface Vanadium Oxide Species on Oxide Supports. *Appl Catal A Gen* **1997**, *157* (1–2), 67–90. https://doi.org/10.1016/S0926-860X(97)00021-5.
(50) Reddy, E. Preparation, Characterization, and Activity of Al2O3-Supported V2O5 Catalysts. *J Catal* **2004**, *221* (1), 93–101. https://doi.org/10.1016/j.jcat.2003.07.011.
(51) Weckhuysen, B. M.; Keller, D. E. Chemistry, Spectroscopy and the Role of Supported Vanadium Oxides in Heterogeneous Catalysis. *Catal Today* **2003**, *78* (1–4), 25–46. https://doi.org/10.1016/S0920-5861(02)00323-1.

Appendix

A. I. 1 Complementary Figures Chapter 1

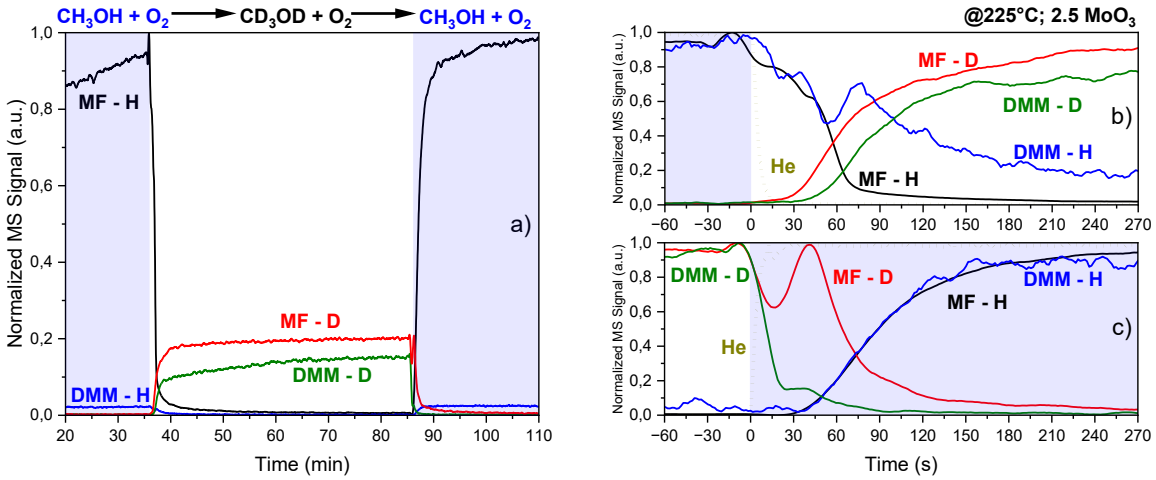

Fig. A.I–1 Normalized MS signal of methyl formate (MF) and dimethoxymethane (DMM), fully hydrogenated (H) and deuterated (D), a) $CH_3OH/O_2/N_2/Ar/He \rightarrow CD_3OD/O_2/N_2/Ar \rightarrow CH_3OH/O_2/N_2/Ar/He$ transition over 2.5 MoO_3/TiO_2 catalyst at 225°C, b) zoom of $CH_3OH \rightarrow CD_3OD$ transition and c) zoom of $CD_3OD \rightarrow CH_3OH$ transition.

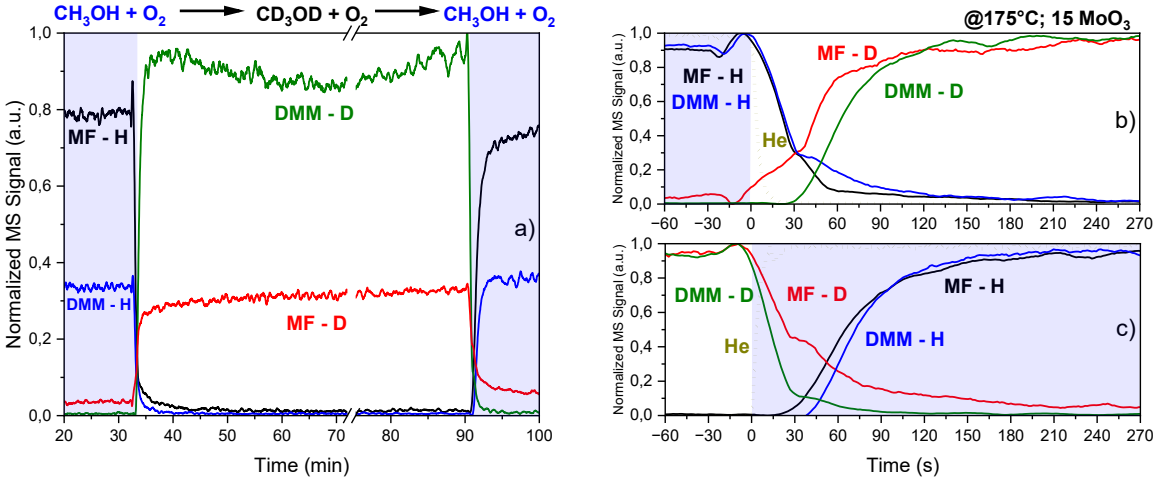

Fig. A.I–2 Normalized MS signal of methyl formate (MF) and dimethoxymethane (DMM), fully hydrogenated (H) and deuterated (D), a) $CH_3OH/O_2/N_2/Ar/He \rightarrow CD_3OD/O_2/N_2/Ar \rightarrow CH_3OH/O_2/N_2/Ar/He$ transition over 15 MoO_3/TiO_2 catalyst at 175°C, b) zoom of $CH_3OH \rightarrow CD_3OD$ transition and c) zoom of $CD_3OD \rightarrow CH_3OH$ transition.

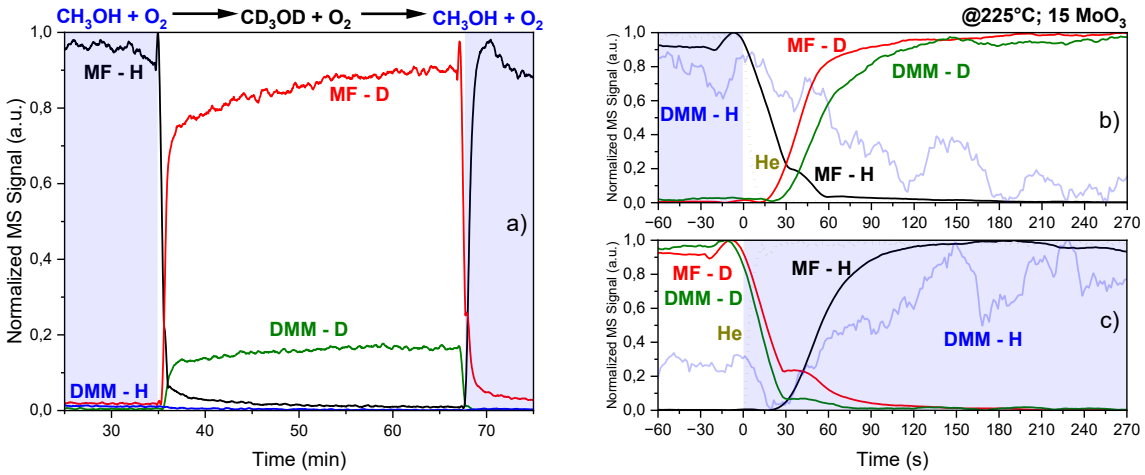

Fig. A.I–3 Normalized MS signal of methyl formate (MF) and dimethoxymethane (DMM), fully hydrogenated (H) and deuterated (D), a) $CH_3OH/O_2/N_2/Ar/He \rightarrow CD_3OD/O_2/N_2/Ar \rightarrow CH_3OH/O_2/N_2/Ar/He$ transition over 15 MoO_3/TiO_2 catalyst at 225°C, b) zoom of $CH_3OH \rightarrow CD_3OD$ transition and c) zoom of $CD_3OD \rightarrow CH_3OH$ transition.

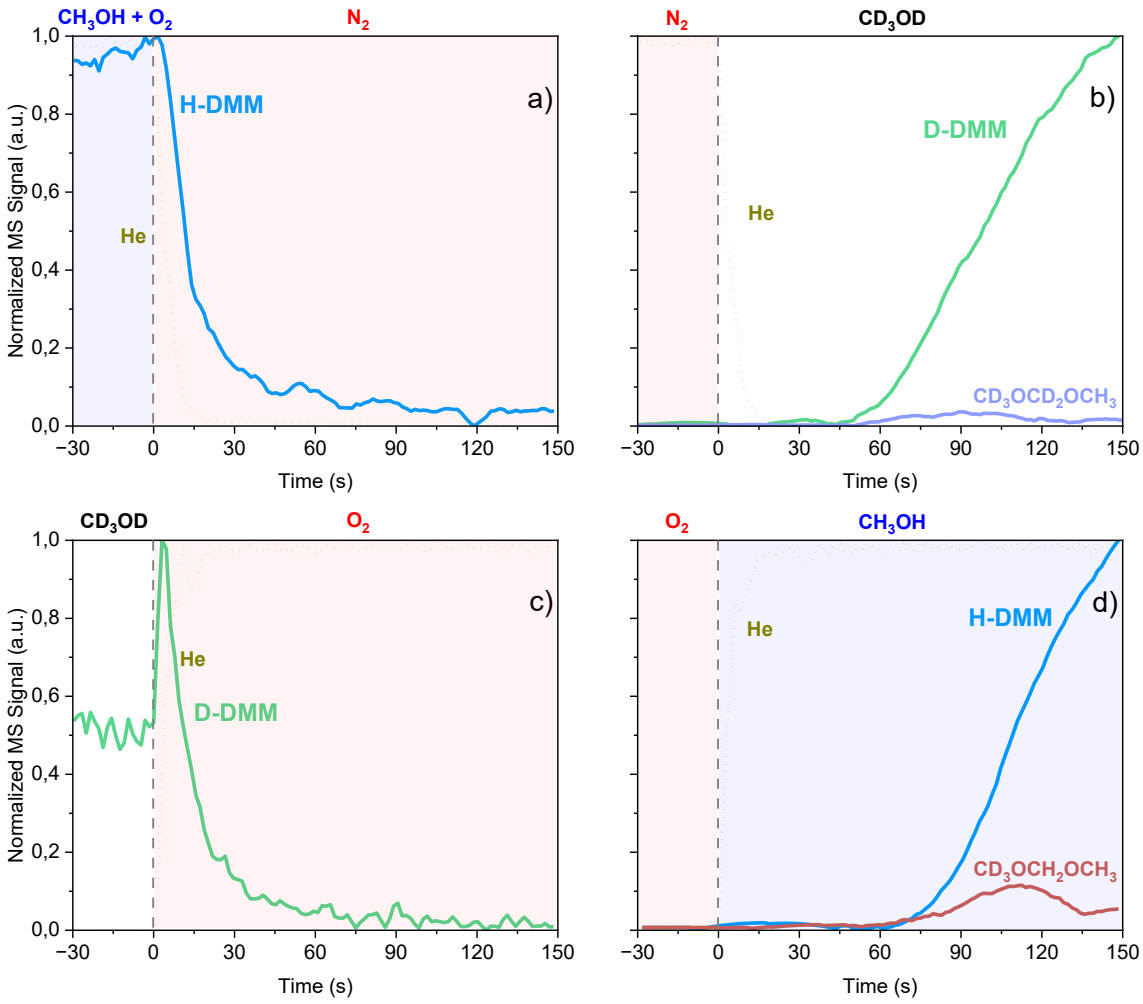

Fig. A.I–4 Normalized MS signal hydrogenated dimethoxymethane ($CH_3OCH_2OCH_3$, H-DMM) and its partially ($CH_3OCH_2OCD_3$) and fully deuterated ($CD_3OCD_2OCD_3$, D-DMM) homologues during the transition a) $CH_3OH + O_2 \rightarrow N_2$; b) $N_2 \rightarrow CD_3OD$ c) $CD_3OD \rightarrow O_2$; d) $O_2 \rightarrow CH_3OH$ at 175°C for the 2.5 MoO_3 catalyst.

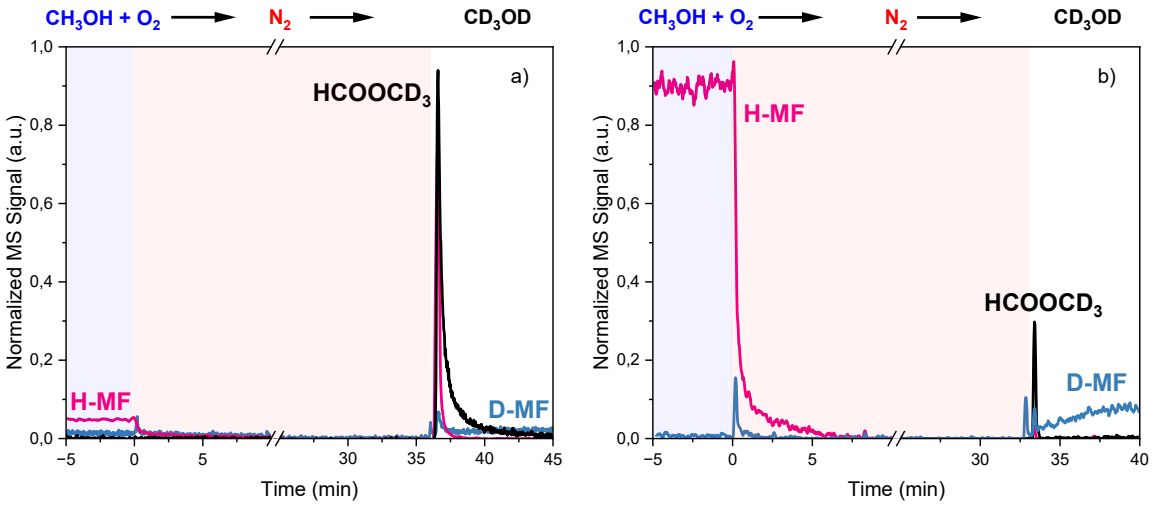

Fig. A.I–5 Normalized MS signal hydrogenated methyl formate ($HCOOCH_3$, H-MF) and its partially ($HCOOCD_3$) and fully deuterated ($DCOOCD_3$, D-MF) homologues during the transition $CH_3OH + O_2 \rightarrow N_2 \rightarrow CD_3OD$ at 175 °C over a) 2.5 MoO_3/TiO_2 catalyst and b) 15 MoO_3/TiO_2 catalyst.

A. I. 2 Analysis of Methoxy Formation Rates and Assessment of Possible Methoxy Exchange

To evaluate whether a methoxy exchange could take place between $HCOOCH_3$ and CD_3OD during the $CH_3OH/O_2/N_2/Ar/He \rightarrow CD_3OD/O_2/N_2/Ar$ transition (or vice versa), an additional analysis was conducted. This question arises from the formation of the partially deuterated methyl formate isotopologue ($HCOOCD_3$), whose origin could, in principle, involve an exchange between hydrogenated and deuterated methoxy species. To assess this possibility, it is necessary to compare conditions where $HCOOCD_3$ is formed, both with and without prior methanol feeding.

Figure A.I–6 compares the formation of surface methoxy species when methanol is fed in the following cases: Fig. A.I–6.a analyzes the rise of the 2925 cm^{-1} band (hydrogenated methoxy) during the $CD_3OD \rightarrow CH_3OH$ transition from the first experiment and the $O_2 \rightarrow CH_3OH$ transition from the second experiment, both at the same temperature on 2.5 MoO_3 catalyst. Conversely, Fig. A.I–6.b displays the $CH_3OH \rightarrow CD_3OD$ transition and $N_2 \rightarrow CD_3OD$ transition, both analyzed through the evolution of deuterated methoxy band (2064 cm^{-1}). The initial slope of these signals was used to estimate the respective formation rate.

The results in both Figures confirm the absence of methoxy exchange, as the surface formation rates remain essentially unchanged. Figure A.I–6.b shows essentially the same rate, while in Fig. A.I–6.a the rate in $CD_3OD \rightarrow CH_3OH$ is slightly slower compared to $O_2 \rightarrow CH_3OH$, which can be rationalized by the need for hydrogenated intermediates to remove

deuterated methoxy already accumulated on the surface, due to higher surface coverage of these deuterated species as mentioned earlier. If there were exchange between methoxy groups, the formation rates should differ between the experiments. In fact, in the first transient experiment methanol was switched under steady state conditions, leading to the simultaneous coexistence of CH_3O^* and CD_3O^* (also CH_3OH, CD_3OD, $HCOOCH_3$). In the second experiment, since a purge or oxidation step consumed methoxy from the previous stage, no interaction allowing methoxy exchange was possible, considering also that $HCOOCH_3$ and $DCOOCD_3$ decrease in the same step that the methoxy disappears from the surface. Therefore, since the methoxy formation rate are similar under conditions where exchange could occur and where it could not, the possibility of methoxy exchange during the $CH_3OH \rightarrow CD_3OD \rightarrow CH_3OH$ sequence is quantitively ruled out. It is worth noting that this analysis is not possibly in the 15 MoO_3 catalyst because during the second transient experiment, the surface was cleaned and there is no discernible detection of $HCOOCD_3$.

Since methoxy exchange was ruled out during the $CH_3OH/O_2/N_2/Ar/He \rightarrow CD_3OD/O_2/N_2/Ar$ transition experiment, a strong argument can be made to discard the Tishchenko reaction pathway on the 2.5 MoO_3 catalyst, where such a route was plausible due to the presence of exposed titania. Therefore, dioxymethylene-formate and hemiacetal pathways should be considered to explain the oxidative dehydrogenation of methanol over MoO_3/TiO_2 catalysts.

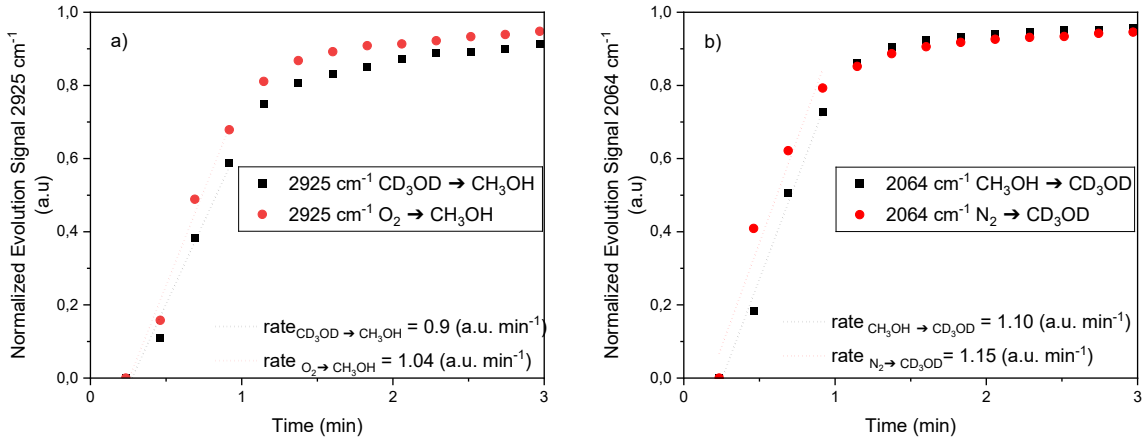

Figure A.I–6 Normalized IR signal of the evolution of the a) hydrogenated methoxy (2925 cm^{-1}) and b) deuterated methoxy (2064 cm^{-1}) on the surface of the 2.5 MoO_3 catalyst at 225 °C in different experiments for CH_3OH or CD_3OD feeding, respectively.

A. II. 1 Methanol adsorption calculations

All samples were quantified identically; therefore, the conversion of MS signal to the molar flow of methanol was performed using the same calibration factor. The methanol molar flow as a function of time was calculated as:

$$\dot{n}_{CH_3OH}\ (mol/s) = \frac{MS\ Signal\ (mV) \cdot F_{total}\ (mol/min)}{factor\left(\frac{mV}{molar\ \%\ CH_3OH}\right)} \cdot \frac{1\ min}{60\ s}$$

This equation yields the instantaneous methanol flow rate, $\dot{n}_{CH_3OH}$. To obtain the total amount of methanol adsorbed on each catalyst, the area under the $\dot{n}_{CH_3OH}(t)$ curve was integrated over time:

$$n_{CH_3OH,ads} = \int \dot{n}_{CH_3OH}(t)\ dt$$

The percentage of exposed TiO_2 for each catalyst is obtained by comparing the total CH_3OH adsorbed on the sample with that adsorbed on the reference TiO_2 (assumed to represent a fully TiO_2 exposed surface):

$$\%TiO_2{}^{Exposed} = \frac{n_{CH_3OH,ads}\ (sample)}{n_{CH_3OH,ads}\ (TiO_2)} \cdot 100\%$$

The surface density of VO_x (expressed as V atoms per nm^2) is computed from the vanadia loading, molar mass, and the available catalyst surface area (corrected for TiO_2 surface loss):

$$\rho_{s-VO_x}\left(\frac{VO_x}{nm^2}\right) = \frac{2 \cdot \left(wt\%\ V_2O_5\left(\frac{g_{v_2o_5}}{g_{cat}}\right)\right) \cdot \left(\frac{1}{181.9} \cdot \frac{mol_{v_2o_5}}{g_{v_2o_5}}\right) \cdot N_A}{\left(1 - \left(\frac{\%TiO_2{}^{Exposed}}{100}\right)\right) \cdot S_{BET}\left(\frac{m^2}{g_{cat}}\right) \cdot 10^{-18}\left(\frac{nm^2}{m^2}\right)}$$

Notes: factor 2 converts V_2O_5 moles to V atoms.

Use the calculated ρ_{s-VO_x} (V/nm^2) to assign the contributions following the adopted regime thresholds.

Regime A: Monomeric and polymeric (no crystalline phase)

If $V/nm^2 < 7.0$, assume no crystalline phase, then:

$$\rho_{s-VO_x} = \rho_{s-monomer} + \rho_{s-polymer}$$

To separate these two contributions, the empirical relation proposed by Broomhead et al.[24] is applied:

$$\rho_{s-VO_x} = \left(\frac{\rho_{s-monomer}}{\rho_{s-VO_x}} \cdot 2.3 \frac{V}{nm^2}\right) + \left(\frac{\rho_{s-polymer}}{\rho_{s-VO_x}} \cdot 7.0 \frac{V}{nm^2}\right)$$

These two empirical anchors allow solving the system of equations to obtain $\rho_{s-monomer}$ and $\rho_{s-polymer}$.

Regime B: Polymeric and crystalline coexistence

If $7.0 < V/nm^2 < 23.4$, assume crystalline phase begins above 11.7 V/nm^2, which corresponds to the maximum density achievable by polymeric VO_x (empirical thresholds)

$$\rho_{s-crystal} = \rho_{s-VO_x} - 11.7 \frac{V}{nm^2}$$

$$\rho_{s-polymer} = 11.7 \frac{V}{nm^2} - \rho_{s-crystal}$$

Ensure $\rho_{s-polymer} \geq 0$; if negative, adjust thresholds or treat as Regime C.

Regime C: Predominantly crystalline

If $V/nm^2 > 23.4$, neglect the polymeric contribution (assumed occluded by crystals) and take:

$$\rho_{s-crystal} = \rho_{s-VO_x} - 11.7 \frac{V}{nm^2}$$

The 23.4 V/nm^2 limit corresponds to the atomic density of the fully crystalline V_2O_5 surface, but operationally the crystalline fraction is defined as the portion exceeding the polymeric maximum.

Using the geometrical stoichiometries assigned to each structural motif (Table II–1), compute the density of each oxygen type:

$$\rho_{s-O^I} = (3 \cdot \rho_{s-monomer}) + (1 \cdot \rho_{s-polymer}) + (0 \cdot \rho_{s-crystal})$$

$$\rho_{s-O^{II}} = (0 \cdot \rho_{s-monomer}) + (4 \cdot \rho_{s-polymer}) + (5 \cdot \rho_{s-crystal})$$

$$\rho_{s-O^{III}} = (1 \cdot \rho_{s-monomer}) + (1 \cdot \rho_{s-polymer}) + (0{,}5 \cdot \rho_{s-crystal})$$

These expressions yield the final surface densities (per nm^2) for O^I, O^{II} and O^{III}.

A. II. 2 *Operando*–DRIFTS analysis during the reverse isotopic switch $CD_3OD \rightarrow CH_3OH$

This appendix presents the *Operando*–DRIFTS analysis performed during the reverse isotopic transition ($CD_3OD \rightarrow CH_3OH$), conducted to validate the mechanistic interpretation discussed in the main text. By monitoring the evolution of methyl formate isotopologues together with the corresponding surface methoxy and formate intermediates, this complementary analysis confirms that the kinetic relationships established in Figure II–9 are reproduced under reversed isotopic conditions.

Figure A.II–1 correlates the MS and IR profiles obtained during the reverse transition ($CD_3OD/O_2/N_2/Ar \rightarrow CH_3OH/O_2/N_2/Ar/He$). Fig A.II–1a and A.II–1c reflect the same relationships between products and surface species observed in Fig. II–9c and II–9a, respectively in the principal text, albeit corresponding to different reaction stages due to the reverse direction of the transition. The behavior discussed for Fig. II–9 is consistently reproduced here.

On the other hand, Fig. A.II–1b focuses on the partially hydrogenated isotopologue of MF ($DCOOCH_3$) and the surface species involved in its formation, namely deuterated formates and hydrogenated methoxy groups. Similar to the behavior observed in Fig. II–9b in the main text, the formation of $DCOOCH_3$ proceeds faster than the accumulation of CD_3O* species on the surface, while the decay of deuterated formates follows the same trend as $DCOOCH_3$, albeit with a slight time offset.

Furthermore, consistent with the behavior described in Fig. A.II–1c, the formation of hydrogenated formates correlates closely with the detection of $HCOOCH_3$ in the gas phase, reinforcing the mechanistic interpretation proposed for the reverse transition.

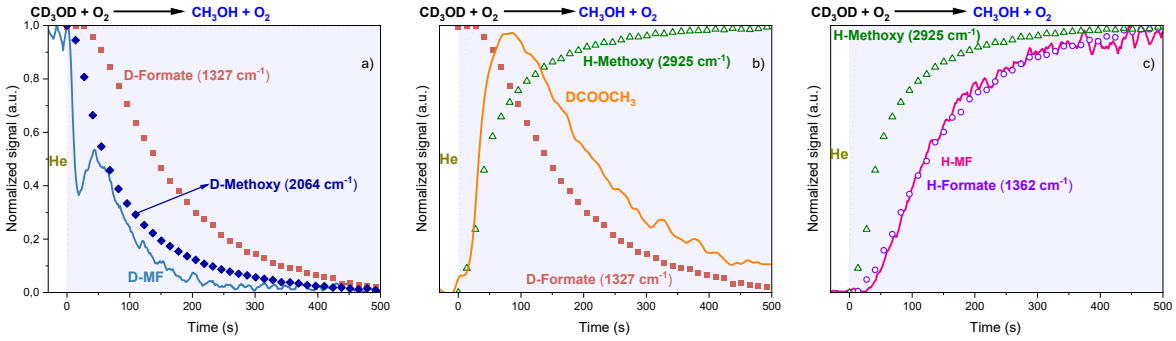

Figure A.II–1 *Operando* IR-MS analysis during the $CD_3OD/O_2/N_2/Ar \rightarrow CH_3OH/O_2/N_2/Ar/He$ transition over the 2.5 V_2O_5/TiO_2 catalyst at 225°C. (a) $DCOOCD_3$ and the evolution of the IR surface species associated with its formation: deuterated methoxy (2064 cm^{-1}) and formate (1327 cm^{-1}). (b) $DCOOCH_3$ and the evolution of the IR surface species associated with its formation: hydrogenated methoxy (2925 cm^{-1}) and deuterated formate (1327 cm^{-1}). (c) $HCOOCH_3$ and the evolution of the IR surface species associated with its formation: hydrogenated methoxy (2925 cm^{-1}) and formate (1362 cm^{-1}).